nature photonics

SUPPLEMENTARY INFORMATION

DOI: 10.1038/NPHOTON.2015.266

# Coordinate-targeted fluorescence nanoscopy with multiple off states

Johann G. Danzl*+, Sven C. Sidenstein+, Carola Gregor, Nicolai T. Urban, Peter Ilgen, Stefan Jakobs and Stefan W. Hell*

Max Planck Institute for Biophysical Chemistry, Department of NanoBiophotonics, Am Fassberg 11, 37077 Göttingen, Germany

+Equal contributors
*Correspondence to
shell@gwdg.de or jdanzl@gwdg.de

DOI: 10.1038/NPHOTON.2015.266

## Image acquisition and analysis

Images were acquired on the home-built microscope using ImSpector software (www.imspector.de). All images represent raw data or, where indicated, raw data slightly smoothed by convolution with a Gaussian using Matlab (Mathworks, Natick, MA, USA). No deconvolution was applied.
For photobleaching experiments (Figs. 2, 3, Suppl. Figs. 3,6), representative images and image series were selected. Bleaching is a sensitive function of the imaging parameters and the fluorophores employed. Results were reproduced several times with the same or similar parameters. Variation of parameters yielded qualitatively similar results. For bleaching experiments, keratin-fluorescent protein fusion constructs were used. Accordingly, fluorophores were not replenished on the timescale of the experiment (minutes). The actin label exhibits a certain degree of turnover.
Imaging parameters and image processing were as follows. Activation was with 405 nm light, unless otherwise noted. Deactivation light was 488 nm continuous wave (*cw)* for the *xy*-doughnut and 491 nm for the *z*-doughnut. Excitation and STED lasers were pulsed lasers with the pulse repetition rate set to 20 MHz and pulse durations of ~100 ps and ~0.7 ns, respectively. The two-photon activation laser was a pulsed fs-laser with 80 MHz repetition rate. Other lasers were *cw* lasers. All laser beams were configured such that they could be switched on and off at defined time points on a µs-timescale relative to the beginning of each scan pixel. Fluorescence was detected with photon-counting avalanche photodiodes. Counts were either registered or rejected by selection on two different timescales. Fluorescence detection was time-gated on a nanosecond timescale, as in conventional gated STED[1]. We applied ns-time-gating both for imaging with protected STED and with plain STED. On the microsecond-timescale of the laser pulse sequence at each scan pixel, fluorescence counts during photoswitching pulses or breaks in the pulse sequence were rejected. The colour maps given with individual images represent the number of single photon counting events detected at individual pixels. Axes designation is *xy* for the focal plane and *z* for the direction along the optical axis (axial direction). All power values given below refer to the power present at the back aperture of the objective lens. The actual power at the sample is lower due to finite transmission of the objective. We estimate the uncertainty in the power measurements to be on the order of 10%.

<u>Parameters for individual images:</u>

**Fig. 2:**
**a,** Living HeLa cell expressing a keratin18-rsEGFP2 fusion protein. The image represents a zoom of the confocal image in panel e of Suppl. Fig. 3. Prior to acquiring this image, the central part of the region shown was first exposed to STED light alone while molecules were in the deactivated state ($OFF_2$), then to STED light alone while molecules resided in the active state and then to excitation plus STED light while molecules were in $OFF_2$. After each exposure, a confocal image was taken (Suppl. Fig. 3). At each scan pixel during the individual rounds of exposure, molecules were subject to the following pulse sequence: photoactivation (50 µs, 210 nW); break (10 µs); excitation (488 nm, 60 µs, 610 nW) and/or STED in *xy*-doughnut geometry (587 nm, 7.1 mW). For experiments with molecules in $OFF_2$, activation light was omitted and molecules in the whole region were first transferred to $OFF_2$ by scanning a larger region with 488 nm light. During each round of exposure, the same region was scanned 4 times and pixel size was 20 nm x 20 nm. Smoothing with a 1.2 pixel wide Gaussian. Blue colour indicates saturation of the colour map at the brightest pixels.
**b,** Confocal image of the same region after additional exposure of the central part to excitation plus STED light with the same parameters as in Fig. 2a but with the additional activation pulse at each scan pixel. Light powers, dwell times, pixel size, smoothing, and colour map were identical to Fig. 2a.
**d,** Pulse sequences at each pixel:
rsEGFP2: photoactivation (50 µs, 280 nW); break (10 µs); deactivation with *xy*-doughnut geometry for variable time (5.3 µW); excitation (488 nm, 30 µs, 2.2 µW) plus STED with *xy*-doughnut (587 nm, 13.1 mW). rsEGFP(N205S): activation (50 µs, 280 nW); break (10 µs); deactivation (3.6 µW); excitation (476 nm, 50 µs, 1 µW) plus STED (587 nm, 3.5 mW). rsEGFP: activation (50 µs, 320 nW); break (10 µs); deactivation (5.3 µW); excitation (488 nm, 50 µs, 1.1 µW) plus STED with *xy*-doughnut geometry (587 nm, 5.1 mW). Pixel size was 20 nm x 20 nm in all cases.

**Fig. 3:**
**a, b,** STED series: activation (40 µs, 140 nW); break (10 µs); excitation (488 nm, 30 µs, 1.4 µW) plus STED with *xy*-doughnut (587 nm, 7.6 mW).

DOI: 10.1038/NPHOTON.2015.266

Protected STED series: activation (50 μs, 210 nW); break (10 μs); deactivation with *xy*-doughnut (350 μs, 4.4 μW); excitation (488 nm, 40 μs, 2.2 μW) plus STED with *xy*-doughnut geometry (587 nm, 1.5 mW).
RESOLFT series: activation (50 μs, 230 nW); break (10 μs); deactivation with *xy*-doughnut (400 μs, 3.7 μW); excitation (491 nm, *cw*, 10 μs, 8.2 μW). We exchanged pulsed excitation at 488 nm for *cw*-excitation at 491 nm, as employed in previous RESOLFT imaging with rsEGFP variants, to exclude the possibility that pulsed excitation could lead to additional photobleaching. Detection was not time-gated on the nanosecond timescale for RESOLFT. Pixel size was 30 nm x 30 nm for each of the series.
Images were smoothed with a 1.2 pixel wide Gaussian.

**Fig. 4:**
**a,** Activation (50 μs, 210 nW); break (10 μs); deactivation with *xy*-doughnut (350 μs, 3.8 μW); excitation (488 nm, 40 μs, 2.1 μW) plus STED with *xy*-doughnut (587 nm, 7.6 mW); break (6 μs). Each line was scanned twice and counts were accumulated. Colour map confocal: 0-50. Raw data smoothed with 1.2 pixel wide Gaussian. Data without smoothing: Suppl. Fig. 10.
**b,** Line profiles were generated with the ImSpector software package on raw data without prior smoothing. An averaging mode was applied that allows setting the width of the region used for line profile calculation. Averaging was set to 10 pixel width. The solid lines represent a fit to the data with a Lorentzian. Fitting was done with the OriginPro software package (OriginLab, Northampton, MA, USA). Signal-to-background ratio was determined between the peak and the immediate surroundings of the respective filament.
**c,** STED: activation (50 μs, 240 nW); break (10 μs); excitation (488 nm, 50 μs, 1.9 μW) plus STED with *xy*-doughnut (587 nm, 11.6 mW). We independently checked that the augmented background observed with STED in comparison with "protected STED" was not due to direct excitation by STED light (anti-Stokes excitation, data not shown). Slight saturation of the colour map range at the thickest structures was tolerated (indicated in blue). RESOLFT: activation (60 μs, 250 nW); break (10 μs); deactivation with *xy*-doughnut (2.5 ms, 5.6 μW); excitation (491 nm, *cw*, 50 μs, 0.7 μW). For this RESOLFT image, we chose continuous wave excitation rather than pulsed excitation to ensure comparability with previously published RESOLFT measurements. Accordingly, no time-gating on the nanosecond timescale was applied. Pixel size: 20 nm x 20 nm.
**e,** Activation (60 μs, 240 nW); break (10 μs); deactivation with *xy*-doughnut (1.5 ms, 4.1 μW); excitation (488 nm, 70 μs, 1.7 μW) plus STED with *xy*-doughnut (587 nm, 6.7 mW). Pixel size: 20 nm x 20 nm.

**Fig. 5:**
**a,** Activation (60 μs, 500 nW); break (10 μs); deactivation simultaneously with *xy*-doughnut (1.5 ms, 2 μW) and *z*-doughnut (1.6 μW); excitation (488 nm, 100 μs, 1.1 μW) plus STED with *xy*-doughnut (572 nm, 7.6 mW) and *z*-doughnut (3 mW). Pixel size: 20 nm x 20 nm. Raw data smoothed with 1.3 pixel wide Gaussian. Data without smoothing are shown in Suppl. Fig. 18. The image colour map was chosen to accurately represent the delicate cortical actin network. The colour map range is saturated at the thickest structures (indicated in white).
**b, c,** Line profiles were generated with the ImSpector software package on raw data without prior smoothing. The averaging width was set to 3 pixels for the bifurcation in panel b and 10 pixels in panel c. The solid lines represent a fit to the data with a single or double Lorentzian, as appropriate for single filaments or bifurcations, respectively. Fitting was done with the OriginPro software package.
**d,** Activation (50 μs, 230 nW); break (10 μs); deactivation simultaneously with *xy*-doughnut (350 μs, 4.4 μW) and *z*-doughnut (491 nm, 2.1 μW); excitation (488 nm, 40 μs, 2 μW) plus STED at 587 nm both with *xy*-doughnut (2.3 mW) and *z*-doughnut (5.8 mW). Data were recorded in *xzy*-scan mode, *i.e.* with the *y*-direction being the slowest scan axis. The image represents raw data smoothed by convolution with a 1.3 pixel wide 2D-Gaussian, first in *xy*- and then in *yz*-direction. The colour lookup table for encoding the third spatial dimension was applied in ImageJ. Voxel size was 35 nm x 35 nm x 55 nm, such that the image corresponds to 36 *z*-slices spaced 55 nm apart. The total imaging volume was 10 μm x 20 μm x 2 μm along the *x*, *y*, and *z*-directions, respectively. Same dataset as in Suppl. Fig. 17.
**e,** Activation (20 μs, 680 nW); break (3 μs); deactivation of rsEGFP(N205S) with *xy*-doughnut (30 μs, 4.1 μW); readout period 1: excitation at 476 nm (30 μs, 1.7 μW) plus STED at 587 nm with *xy*-doughnut (3.4 mW); readout period 2: excitation at 516 nm (30 μs, 0.4 μW) plus STED at 587 nm with *xy*-doughnut geometry (3.4 mW). Fluorescence was detected in two spectral channels at ~490 nm to ~510 nm and ~520 nm to ~565 nm. This resulted in a total of 4 recorded channels. Linear unmixing was performed with ImageJ. The mixing matrix was generated from the same dataset by defining a region that contained only background signal, a region that contained only rsEGFP(N205S)-Rab5a signal and a region that contained only citrine-Map2 signal. After colour separation, images were smoothed by convolution with a 1.3 pixel wide Gaussian. Colour maps confocal: green 0-90 counts; fire 0-60 counts. Colour maps

nanoscopy: green 0-40 counts, fire 0-25 counts. Pixel size: 25 nm x 25 nm for nanoscopy and 30 nm x 30 nm for confocal data.

**Fig. 6:**
Two-photon activation (800 nm, 30 μs, 5.9 mW); break (3 μs); deactivation simultaneously with *xy*-doughnut (180 μs, 7.8 μW) and *z*-doughnut (8.7 μW); excitation (488 nm, 80 μs, 3.4 μW) plus STED with *xy*-doughnut (3.5 mW) and *z*-doughnut (2.1 mW) at 587 nm. Voxel size was 35 nm x 35 nm x 80 nm. The total imaging volume was 7 μm x 20 μm x 4.5 μm in *x*, *y*, and *z*-directions, respectively. The volume was recorded in *xzy*-scan mode. The image represents a 3D-volume rendering done with the Amira software package v6.0 (Hillsboro, OR, USA) after smoothing raw data by convolution with a 1.2 pixel wide three-dimensional Gaussian.

## Cell culture and transfection

CV-1 cells (Invitrogen, Carlsbad, CA, USA) and HeLa cells were cultured in DMEM (Dulbecco's modified Eagle's medium, high glucose, Gibco/Thermo Fisher, Waltham, MA, USA), supplemented with 10 % fetal bovine serum (FBS superior, Biochrom, Berlin, Germany), penicillin/streptomycin (Biochrom), and 1 mM Na-pyruvate (Sigma Aldrich, St. Louis, MO, USA). For imaging, cells were plated on #1.5 glass coverslips and transfected on the next day with Turbofect or Lipofectamine 2000 (Thermo Fisher) according to the manufacturer's instructions. Cells were typically used for imaging 20-48 h after transfection. Imaging was performed in high-glucose DMEM without phenol red or glutamine (Gibco), supplemented with 10 mM Hepes (AppliChem, Darmstadt, Germany) and penicillin/streptomycin.

## Plasmids

For creation of keratin18-rsEGFP and keratin18-rsEGFP2 fusion constructs, the coding sequences of both RSFPs were amplified by PCR reactions (forward primer: GACGGTACCGCGGGCCCGGGATCCACCG GTCGCCACCATGGTGAGCAAGGGCGAGGAGCT; reverse primer GTCGCGGCCGCTTACTTGTACAGCTCGTC). Subsequently the PCR products were cloned into the pTagRFP-keratin vector (Evrogen, Moscow, Russia) using the KpnI and NotI restriction sites to replace the TagRFP coding sequence. The keratin18-rsEGFP(N205S) fusion construct was cloned in the same way but using the forward and reverse primers GACGGTACCGCGGGCCCGGGATCCACCGGTCGCCACCATGGTGAGCAAGGGCGAGGAG and TACCCTGCGGCC GCTTTACTTGTACAGCTCGTCCATGCC, respectively.
The rsEGFP(N205S)- and rsEGFP2-actin affinity labels AC-rsEGFP(N205S) and AC-rsEGFP2 were based on an actin-binding camelid antibody (actin Chromobody, Chromotek, Planegg-Martinsried, Germany) and constituted fusion proteins of the actin Chromobody (AC) and the respective RSFP. They were generated as follows. The actin Chromobody-TagGFP plasmid (pAC-TagGFP, Chromotek) was used as a template to amplify the actin binding domain actin-VHH using the primers GATCGCATGCCTTAAGATGGCAC AGGTTCAGCTG and CTAGGGTACCACCGGTGGCACCACTACCGGAGCTGACTGTCACCTG, introducing recognition sites for the restriction enzymes SphI and KpnI at the 5' and 3'-end, respectively. After digestion with SphI and KpnI, the PCR-fragment was cloned into the plasmid pQE30 (Qiagen, Hilden, Germany) resulting in the plasmid pQE30-AC. The rsEGFP(N205S) and rsEGFP2 coding sequences[2,3] were amplified using the primers CTAGCTGCAGCCACTAGTGGTAGTGGTGCCATGGTGAGCAAGGGCGAG and TCGAAAGCTTTTACTTGTACAGCTCGTCC, digested with PstI and HindIII and cloned into pQE30-AC, generating the bacterial expression plasmids pQE30-AC-rsEGFP(N205S) and pQE30-AC-rsEGFP2. To create the mammalian expression plasmids pAC-rsEGFP(N205S) and pAC-rsEGFP2, the coding sequences for AC-rsEGFP(N205S) and AC-rsEGFP2 were amplified with the primers GATCAGATCTCGATCGATGGCTCAGGTGCAGCTGGT and CTAGGCGGCCGCACCGGTTTACTTGTACAG CTCGTCCATGC. After digestion with BglI and NotI the PCR products were used to replace the coding sequence for AC-TagGFP in pAC-TagGFP. For the creation of AC-rsEGFP2 viral vectors, the coding sequence was amplified with the primers GTACCTCGAGATGGCTCAGGTGCAGCTGGTGGAG and CGATGCGGCCGCTTACTTGTACAGCTCGTCCATGCC, and ligated into the XhoI/NotI opened plasmid pSCA3-Lifeact-YFP[4], resulting in the plasmid pSCA3-AC-rsEGFP2.
The plasmids coding for rsEGFP2-Rab5a and rsEGFP(N205S)-Rab5a were constructed in the following way. RSFP coding sequences were amplified with forward primer CGACGCTAGCATGGTGAGCAAGGGCG and reverse primer GATCCCAAGCTTCTTGTACAGCTCGTC and inserted between NheI and HindIII restriction sites in a pcDNA3.1(+) vector construct that contained a flag tag sequence between the HindIII and BamHI restriction sites. The Rab5a sequence was amplified with primers

DOI: 10.1038/NPHOTON.2015.266

CGCGGATCCAGGCTAGTCGAGGCGCAACAAGA and CATCCGGAATTCTTAGTTACTACAACACTGATT and inserted between BamHI and EcoRI restriction sites.
The citrine-map2 construct was generated with the gateway cloning technique (Invitrogen, Carlsbad, CA). The DNA sequences were fused by recombination between a pSEMS-citrine gateway destination vector for N-terminal tagging and a pDONR223-MAP2 gateway donor vector (CCSB Human ORFeome Collection v5.1)[5]. The plasmids for targeting rsEGFP2 to the endoplasmic reticulum by fusion to KDEL and to peroxisomes by fusion to Pex16 were described previously[3].
The vimentin-rsCherryRev1.4 plasmid was generated by replacing the mKate2 sequence in the mKate2-vimentin plasmid (Evrogen) with the rsCherryRev1.4 coding sequence[6] using restriction sites for AgeI and NotI. Similarly, the keratin-Dronpa(M159T) plasmid was generated by inserting the coding sequence for Dronpa(M159T) with modified N- and C-termini[7] into the TagRFP-keratin18 plasmid using KpnI and NotI. For generating the vimentin-rsEGFP2 plasmid, the rsEGFP2 coding sequence was amplified by PCR and inserted into the pmKate2-vimentin vector (Evrogen) via restriction sites for AgeI and NotI.

## Preparation of cultured hippocampal brain slices

Organotypic hippocampal slice cultures were prepared from wild-type C57BL/6 mice on postnatal day 5-7. Hippocampi were dissected into 400 μm thick slices and each slice was embedded in a plasma clot on a #1 cover slip. The plasma clot was formed using equal parts of chicken plasma (Sigma Aldrich) and a coagulating thrombin solution, which contained 0.5mg/ml thrombin (VWR/Merck, Darmstadt, Germany) resuspended in equal parts of distilled water and Gey's balanced salt solution (home-made, components from VWR/Merck). Slices were cultured in a roller incubator at 35°C according to procedures described by Gähwiler *et al.*[8] in a medium composed of: 97 ml Basal Medium Eagle (Gibco), 50 ml Hank's Buffered Salt Solution (Gibco), 50 ml horse serum (Gibco), 2 ml of 45% glucose solution (VWR/Merck), 1 ml of 200 mM glutamine solution (Gibco). Slices were used for imaging 10 days to ~6 weeks after preparation.
Semliki Forest virus particles (SFVs) for expression of AC-rsEGFP2 in living brain slices were generated essentially as previously described[4]. We incorporated the DNA sequence coding for a fusion protein of the actin chromobody with rsEGFP2 into a pSCA3 vector as described above. We cotransfected Hek293 cells with the pSCA3-AC-rsEGFP2 plasmid and a pSCA helper plasmid coding for viral structural components[9]. Five days after transfection, we lysed cells with two freeze-thaw cycles. Cellular debris was removed by centrifugation at 1,700 g for 10 minutes. SFVs were pelleted by centrifugation at 48,000 g for 2 hours and resuspended in TBS-5 (130 mM NaCl, 10 mM KCl, 5 mM $MgCl_2$, 50 mM Tris-HCl, pH 7.8). Chymotrypsin was applied for virus activation.
Virus particles were injected into the CA1 and CA3 regions with a pressure injector (Tooheyspritzer, Toohey Company, Fairfield, NJ) using a patch clamp pipette. Slices were cultured for another 12 – 48 h after virus injection. Slices were transferred to an imaging chamber and imaged in artificial cerebrospinal fluid containing 126 mM NaCl, 2.5 mM KCl, 2.5 mM $CaCl_2$, 1.3 mM $MgCl_2$, 30 mM glucose, 27 mM Hepes with pH adjusted to 7.4 with NaOH. Imaging was performed at room temperature.

## Suppl. Figure 1: State diagram for protected STED with rsEGFP variants

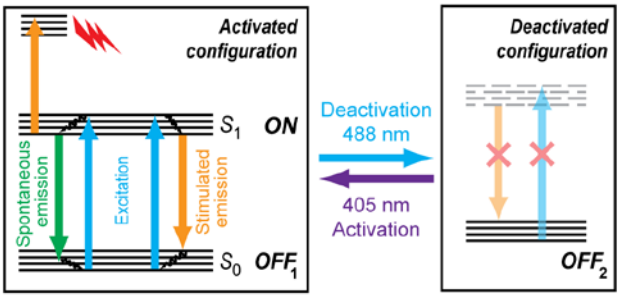

## Suppl. Figure 2: Home-built 3D-protected STED setup

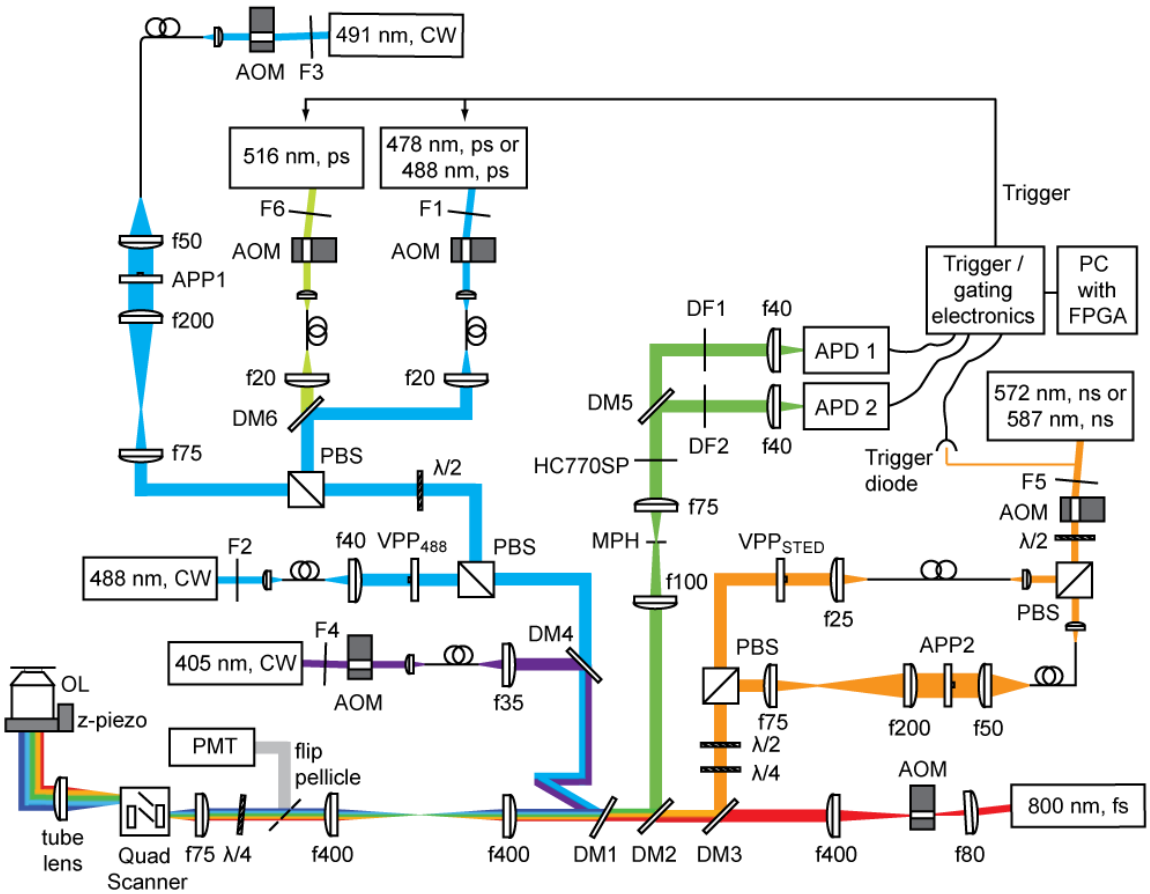


Transfer to the deactivated state $OFF_2$ was accomplished with light from a 488 nm continuous wave (*cw*) diode laser (LBX-488-70-CIR-PP, Oxxius, Lannion, France) passed through a polymer vortex phase plate $VPP_{488}$ (VPP1a, RPC Photonics, Rochester, NY, USA, 487 nm vortex mask). This generated a 2π-helical phase modulation of the beam, giving rise to a doughnut-shaped beam in the microscope's focus and resolution enhancement in the focal plane (hence the term "*xy*-doughnut geometry"). In addition, light from a 491 nm DPSS laser (Dual Calypso, Cobolt, Solna, Sweden), with external power modulation by an acousto-optical modulator (AOM) (3080-125, CrystalTechnologies, EQPhotonics, Eching, Germany), was passed through a home-made annular phase plate (APP1) to generate a "*z*-doughnut" pattern with a central intensity minimum and intensity maxima above and below the focal plane, leading to resolution enhancement along the optical axis. Measured point-spread-functions are given in Suppl. Fig. 17. A $MgF_2$ disc of 4.2 mm diameter and ~680 nm thickness on BK7 substrate was used in conjunction with a 100x oil objective for 3D-subdiffraction imaging of living cultured cells. In combination with a 63x glycerol objective for 3D-subdiffraction imaging of living brain slices, a 5.8 mm diameter cryolite layer of ~810 nm thickness was chosen. Activation light stemmed from a 405 nm Toptica DL100 *cw* diode laser passed through 2 AOMs for maximum extinction. Some experiments were carried out with a 405 nm diode laser from Oxxius (405-100-COL). STED light was generated by a pulsed Raman-shifted fibre laser (Rainbow prototype system, IPG Photonics, Mountain View, CA, USA) with a pulse repetition rate between 1 and 20 MHz. All data shown were recorded with 20 MHz repetition rate, unless specifically noted. For the present experiments, we chose either 572 nm or 587 nm as STED wavelength. For the experiments in Suppl. Fig. 15, the STED wavelength was set to 558 nm. The pulse width was set between 500 ps and 1.1 ns. The output of the STED laser was passed through an AOM (AA MT110-1.5-VIS, AA Opto-electronic, Orsay, France), split, and delivered to the setup via two separate polarization-maintaining single mode fibres of equal length for the *xy*-doughnut and the *z*-dougnut, respectively. For the STED doughnut generating resolution enhancement in the *xy*-plane, a helical phase pattern was imprinted on the beam by the vortex phase plate $VPP_{STED}$. For 572 nm STED wavelength, we used a VPP1a phase plate from RPC

DOI: 10.1038/NPHOTON.2015.266

Photonics and chose the 596 nm vortex for $VPP_{STED}$. For 587 nm STED wavelength, we used a VPP1b vortex phase plate, employing the 582 nm vortex. The z-doughnut for STED with the 100x oil immersion objective was generated with a home-made annular phase plate APP2 consisting of a $MgF_2$ disk of 4.1 mm diameter and ~700 nm thickness on BK7 substrate. For STED at 587 nm with the 63x glycerol objective, the *z*-doughnut was created with a 4.9 mm diameter cryolite disk of ~840 nm thickness on a glass substrate. Excitation pulses were provided by diode lasers with ~100ps pulse length. We either used a 488 nm PicoTA (Toptica Photonics, Graefelfing, Germany and PicoQuant, Berlin, Germany) or a LDH-D-C-485 with emission at 476 nm (PicoQuant, Berlin, Germany). Excitation lasers were passed through AOMs (MT110-A1-VIS or MT200-A0.5-VIS, AA Opto-electronics) for intensity modulation and switching. Light for two-photon activation was delivered by a MaiTai-HP titanium:sapphire femtosecond laser (Newport-Spectra Physics, Santa Clara, CA, USA), intensity modulated by an AOM (MT110-A1-IR, AA Opto-electronics). Laser beams were overlapped on dichroic mirrors (DM) or polarizing beamsplitter cubes (PBS, B. Halle, Berlin, Germany). Beam scanning was accomplished with a home-built scanner ("Quad-Scanner") including 4 galvanometer scan mirrors. A tube lens (TL) from Leica Microsystems (Wetzlar, Germany) was used. For experiments with living cultured cells, we used a Leica 100x plan-apo oil-immersion objective lens (HCX-PL-APO 100x/1.4-0.7 OIL CS). For experiments with living hippocampal brain slices, we used a 63x glycerol objective (HC PL APO 63x/1.3 GLYC CORR CS2, Leica). For fine focus control and scanning in the axial direction, the objective lens (OL) was moved along the optical axis with a piezo translator (*z*-piezo, Mipos 100PL CAP, Piezosystem Jena, Jena, Germany). Fluorescence was collected with the same objective lens, descanned, and imaged onto a pinhole of variable size (MPH16, Thorlabs, Newton, NJ, USA). Pinhole size was chosen to correspond to 0.7 - 1.0 x the diameter of the Airy disk at the location of the pinhole. For the experiments in Fig. 6, pinhole size corresponded to ~1.24 Airy disks. Fluorescence was filtered with a BrightLine 525/50 filter (DF1, Semrock, Rochester, NY, USA, angle tuned for maximum photon collection) and detected with an avalanche photodiode (SPCM-AQRH-13, Excelitas, Waltham, MA, USA or PDM module from MPD, Bolzano, Italy). For some of the experiments, we split the fluorescence signal with a dichroic mirror (DM5, Razor Edge 514, Semrock) onto two APDs, with a BrightLine 535/50 and optionally a 594 nm notch filter in the second channel (DF2, Semrock). The two detectors in parallel allowed higher peak photon count rates and slightly extended the spectral range detected. For the two-colour experiments in Fig. 5e, the short wavelength channel was filtered with BrightLine 514/30 and StopLine 532 filters. Both filters were angle tuned to adjust transmission and blocking bands. The long wavelength channel was filtered with a BrightLine 535/50 filter in combination with an EdgeBasic 514 long wave pass filter. Excitation for two-colour experiments was either with a single laser at 476 nm or 488 nm or with a combination of the 476 nm laser and a 516 nm pulsed laser diode (LDH-D-C-510, PicoQuant, Berlin, Germany) for selective excitation of citrine. The 516 nm laser was coupled into the experiment via dichroic mirror DM6 (495DCXRU, Chroma, Bellows Falls, VT, USA). For experiments involving 2-photon activation of RSFPs, we added a HC770SP (Chroma) blocking filter. Light from the lasers was passed through appropriate cleanup filters (F1: BrightLine 488/6 for 488 nm and Semrock Versachrome for 478 nm, F2: Semrock MaxLine 488 F3: 532 nm notch + 491/10, F4: BrightLine 405/10, F5: BrightLine 591/6 plus StopLine 594 for STED at 587 nm and Bright Line 575/15 plus StopLine 594 for STED at 572 nm, F6: BrightLine 520/5) and delivered to the setup via polarization-maintaining single-mode fibers with the exception of the femtosecond 2-photon activation laser. DM1: 460DCXRU (angle tuned, Chroma). DM2: 565DCXRU (Chroma). DM3: ZT594RDC (Chroma). DM4: 450DCXRU (Chroma). For alignment, a pellicle beam splitter (BP145B1, Thorlabs) was flipped into the beam path to direct light reflected by the alignment sample onto a photomultiplier tube (PMT, H10723-01, Hamamatsu Photonics, Hamamatsu, Japan) or a webcam. In the figure, beam steering mirrors and some parts of the setup that are not relevant for the present experiments were omitted for clarity. STED laser pulses were sampled and excitation pulses were triggered and synchronized to the STED laser by home-built electronics. Optical and electronic delays were chosen such that synchronization was on a pulse-to-pulse basis to render any pulse-to-pulse timing jitter of the STED laser irrelevant and to allow flexible tuneability of the STED and excitation laser repetition rates. Fluorescence detection for nanoscopy images was time-gated on a nanosecond timescale, unless otherwise noted. Time-gating of the APD signal was accomplished by home-built electronics. Experiment control and image acquisition were done with the ImSpector software. Hardware control was accomplished via an FPGA board (PCIe-7852R, National Instruments, Austin, TX, USA). For experiments involving two APDs, the second APD was time-gated on the FPGA-board.

**Beam alignment**

For protected STED imaging, the intensity minima of the beams for photoswitching to $OFF_2$ and for STED must be overlapped precisely. We found that using an alignment sample prior to imaging for overlapping the "zeros" with the signal from gold or silver nanospheres detected on the PMT was sufficient for

satisfactory imaging results. We initially cross-checked alignment with fluorescent nanospheres. For 3D-subdiffraction imaging in living tissue, we found that adjustment of the correction collar of the glycerol objective to compensate for spherical aberration at a particular imaging depth and subsequent overlapping of the intensity minima resulted in sufficient alignment quality.

**Setup for testing the protective effect of transfer to deactivated state in the red spectral region**

For experiments with rsCherryRev1.4 (Suppl. Fig. 6), we exchanged the STED laser for a 775 nm pulsed laser operating at 20 MHz repetition rate with 1.2 ns pulse duration (ELP-5-775-DG, IPG Photonics Corporation, Oxford, MA, USA). Activation light stemmed from a 440 nm pulsed laser diode (LDH-P-C440B, PicoQuant) and excitation light at 560 nm was derived from a supercontinuum laser source (Solea, PicoQuant) synchronized on a pulse-to-pulse basis to the STED laser. Deactivation light was derived from a 592 nm *cw* laser (VFL-P-1000-592, MPB Communications, Montreal, Canada). All lasers were passed through acousto-optical devices to enable power regulation and switching relative to the start of each scan pixel. All laser beams were regularly focused by the objective lens and produced near diffraction-limited PSFs. Fluorescence was detected in the 600 nm – 650 nm spectral window.

DOI: 10.1038/NPHOTON.2015.266

## Preconditions for protected STED imaging

The specific requirements for the combination of two or more state transitions fall into three broad categories: (I) driving a transition between two states must not lead to loss by acting on a third state, (II) transitions must be sufficiently decoupled, and (III) action of one off-transition must not impede action of other off-transitions. These are tested in Suppl. Fig. 3-5.
Transitions do not need to be fully decoupled for MOST nanoscopy. For example, a situation would be desirable where STED light additionally drives protective transfer ($OFF_1 \rightarrow OFF_2$). We employed fluorophores where excitation is coupled to transfer to the deactivated state ("negative" switching behaviour). However, fluorophores that feature "positive" switching (where excitation light leads to activation of fluorophores) should be amenable to protected STED nanoscopy as long as the timescales of fluorescence readout and fluorophore activation can be separated.

## Suppl. Figure 3: STED light does not cause loss of molecules from $OFF_2$

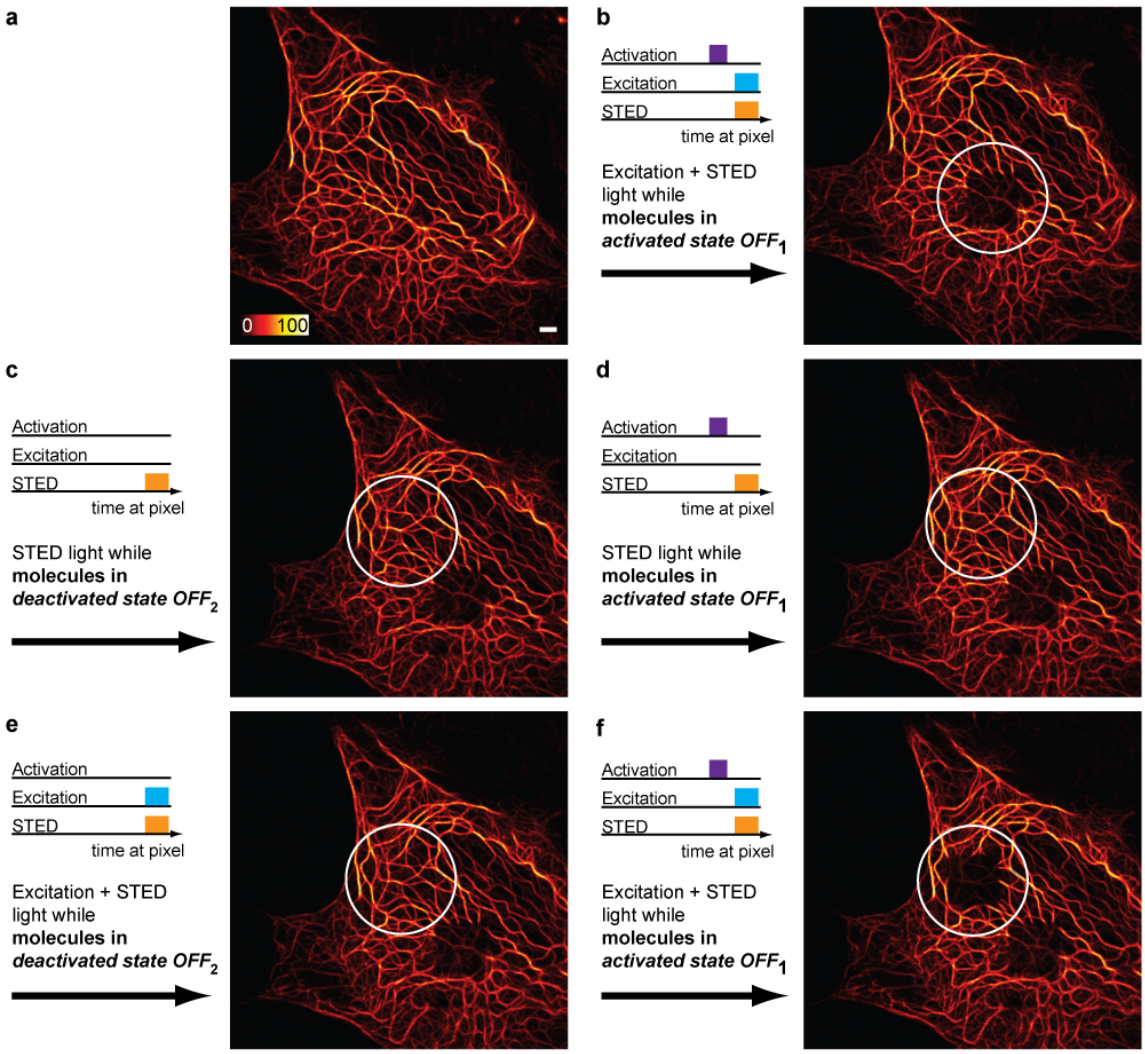


Confocal image series of the same cell as in Fig. 2a,b, expressing a keratin-rsEGFP2 fusion protein. **a,** Reference image without prior light exposure. **b,** Confocal image after repeatedly scanning a square region within the white circle with excitation and STED light while molecules were in the activated state (*i.e.* including an activation light pulse at each scan pixel, as shown in the schematic). This corresponds to light exposure during conventional STED imaging and led to pronounced photobleaching of the exposed area. **c,** Confocal image after scanning a different region of the cell within the white circle with only STED

light while molecules were in the deactivated state. For this, molecules were first transferred to $OFF_2$ by scanning a large region with 488 nm *cw* light and the photoactivation pulse at individual scan pixels was omitted. The absence of prominent bleaching indicates that STED light does not lead to loss out of the state system by adversely affecting molecules in $OFF_2$. **d,** Same measurement, but after exposure of molecules to STED light while they resided in $OFF_1$. Again, no unexpected bleaching took place. **e,** Confocal image after exposing molecules in $OFF_2$ to excitation plus STED light. This situation corresponds to the light exposure in high STED intensity regions during protected STED imaging. The absence of prominent bleaching indicates that transfer to $OFF_2$ is protective. Fig. 2a is an enlarged view of the exposed region in this image. **f,** Confocal image after exposure of molecules in the activated state to excitation and STED light. Again, prominent bleaching is observed (same data as in Fig. 2b). For parameters see Fig. 2a,b. Scale bar: 2 μm.

## Suppl. Figure 4: STED light does not significantly photoactivate rsEGFP variants in protected STED imaging.

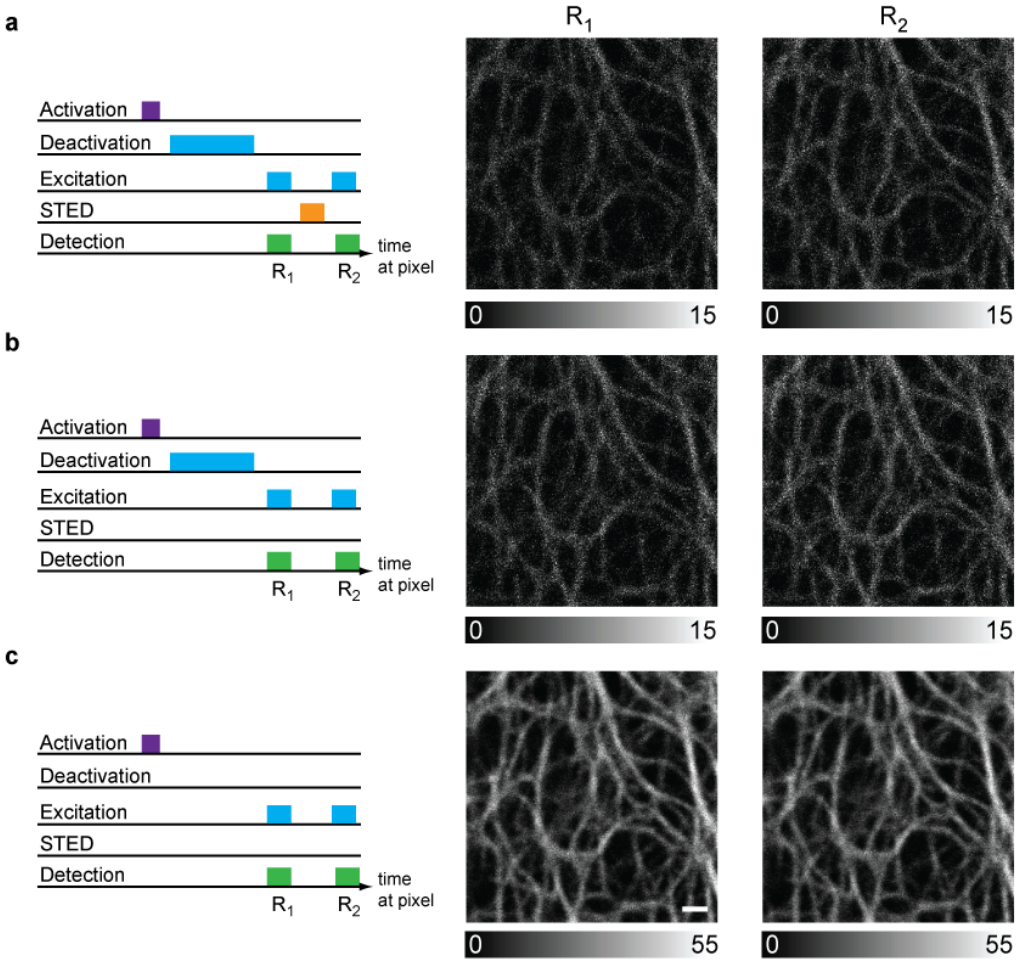


**a,** A living HeLa cell expressing a keratin-rsEGFP(N205S) fusion protein was imaged with the indicated sequence of light pulses at each scan pixel. After activation, fluorophores in the focal region were deactivated by irradiating with a regularly focused and a doughnut beam simultaneously. Fluorescence excited during a first readout period $R_1$ thus represented "photoswitching background". Then a pulse of STED light (without excitation light) was applied to test whether STED light would drive the $OFF_2 \rightarrow OFF_1$ transition. During the second readout period $R_2$, identical excitation parameters as for $R_1$ were applied. The two panels on the right correspond to the two separate readout periods $R_1$ and $R_2$. Mean counts per pixel were slightly higher in $R_2$ than in $R_1$ (1.8 and 1.5, respectively). This observation is in contrast to the expected large increase in fluorescence between $R_1$ and $R_2$ in case STED light would cause significant photoactivation. **b,** To test whether the slight increase in brightness was caused by action of STED light through *e.g.* two-photon activation, we repeated the experiment omitting the STED pulse. A similarly

DOI: 10.1038/NPHOTON.2015.266

increased mean count per pixel was evident in $R_2$ vs. $R_1$ (2.1 and 1.8, respectively). Hence, the increase in fluorescence likely represents a return of molecules from dark states populated during photoswitching and/or thermal relaxation from $OFF_2$ to $OFF_1$. In rsEGFP variants, the activated state is the thermal equilibrium state. **c,** Confocal reference image recorded with only activation and readout pulses applied at individual scan pixels. Fluorophores resided in the activated state during $R_1$ and $R_2$. Mean counts per pixel were 12.1 and 11.8 for $R_1$ and $R_2$, respectively. Here, excitation power was one quarter of that applied in panels a,b. A slight decrease in fluorescence counts is expected between readout periods $R_1$ and $R_2$ because of partial photoswitching to $OFF_2$ by excitation light.
The fluorescence count ratio for readout period $R_1$ between panels a and c and between panels b and c is 0.12 and 0.15, respectively. Taking the different excitation powers into account by linearly scaling up counts in panel c, this corresponds to ~3-4% photoswitching background in panels a and b, which is a typical value for rsEGFP(N205S). The increase in fluorescence observed between $R_1$ and $R_2$ in panels a and b is negligible compared to the decrease in fluorescence achieved with photoswitching to $OFF_2$. Both for panel a and b, the signal increase between $R_1$ and $R_2$ amounts to ~0.7 % of the signal modulation achieved through photoswitching, evaluated between $R_1$ of the respective panel and $R_1$ in panel c. In contrast to the measurements presented here, including deactivation light pulses at each pixel, we observed that it is possible to at least partially activate molecules if the accumulated STED light exposure is increased to levels that by far exceed those that would be experienced by molecules in a protected STED imaging situation.

Parameters:
**a,** Activation (50 μs, 300 nW); break (10 μs); deactivation simultaneously with a regularly focused beam (491 nm, *cw*, 2 ms, 3.8 μW) and a doughnut beam (4.4 μW); $R_1$ with excitation by regularly focused beam (488 nm, 50 μs, 1.1 μW); break (1 μs); STED light with regularly focused beam (587 nm, 50 μs, 3.5 mW); break (1 μs); $R_2$ with excitation by regularly focused beam (488 nm, pulsed, 50 μs, 1.1 μW). The choice of power for the STED beam reflects the fact that for given total power the peak intensity in a regularly focused, diffraction-limited beam is about 3 times the peak intensity in doughnut geometry. A regularly focused rather than doughnut geometry was chosen for the STED beam in order to ensure maximum overlap with the excitation and confocal detection volumes. **b,** Identical parameters as in panel a but without the STED light pulse. **c,** Activation (50 μs, 300 nW); break (2.01 ms); $R_1$ (50 μs, 280 nW); break (52 μs); $R_2$ (50 μs, 280 nW). Pixel size was 30 nm x 30 nm in all panels. Scale bar: 1 μm. The colour map is linear. Data are raw.

## Suppl. Figure 5: Deactivation does not impede STED and photoswitching background is removed by STED.

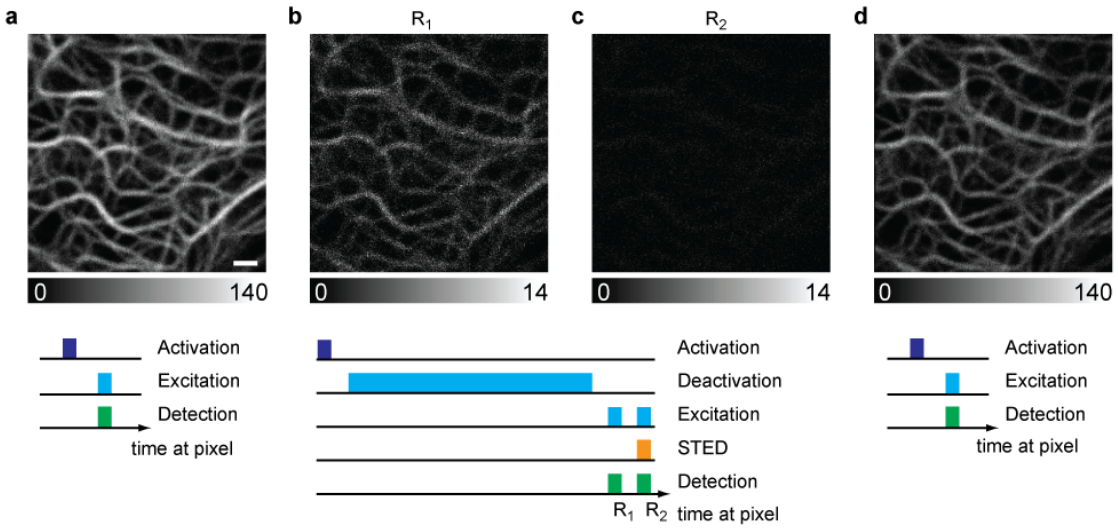


An ensemble of reversibly switchable fluorescent proteins exhibits photoswitching background, *i.e.* some residual fluorescence that can be excited even after applying light for transfer to the deactivated state. Note that photoswitching background reduces state contrast between designated on- and off-regions in single-transition nanoscopy. Here we tested whether spurious signal from photoswitching background

can be counteracted by STED in rsEGFP variants. The residual fluorescence might exhibit altered spectral or fluorescence decay characteristics. This can in principle impede the STED process whose parameters were adjusted to the properties of active-state fluorophores. **a,** Confocal reference image of a living HeLa cell expressing a keratin-rsEGFP(N205S) fusion protein. The sequence of light pulses at each scan pixel is shown below the respective panels. **b, c,** Here, we applied at each scan pixel first an activation pulse and then deactivated molecules in the whole focal volume by ~490 nm light simultaneously with doughnut and regularly focused geometries. Fluorescence detected during application of excitation light in a first readout period $R_1$ (panel b) hence corresponded to RSFP switching background. Note the 10x scaling difference in the colour map with respect to panel a. Switching background was ~2.5% (mean counts per pixel in panel b: 1.6; mean counts per pixel in panel a: 31.6; ratio: 0.05; excitation power in panel a was one half the excitation power in panel b in order to avoid saturation of APDs). In a second readout period $R_2$ (panel c), excitation light was as in $R_1$ and we added STED light with regularly focused and doughnut geometries together to create a spatial light distribution that included the whole focal volume of the excitation laser. Photoswitching background was removed almost completely (mean counts per pixel: 0.4). This resulted in a brightness ratio between panel c and panel a of ~0.6%, taking the reduced excitation power in panel a into account. **d,** Confocal scan recorded after panels b,c with identical parameters as in panel a. Overall counts were ~71 % of counts in panel a, showing moderate bleaching despite application of high STED power in panel c. Scale bar: 1 μm.

Parameters:
**a,** Activation (280 nW, 50 μs); break (10 μs); excitation (488 nm, 500 nW, pulsed, 50 μs). Pixel size: 50 nm x 50 nm. **b,c,** Activation (280 nW, 50 μs); break (10 μs); deactivation with a doughnut beam (4.4 μW) and a regularly focused beam (491 nm, 3.3 μW) for 2 ms; $R_1$ (488 nm, 50 μs, 1 μW); $R_2$ with identical parameters for excitation and additional STED light (587 nm with 10.5 mW *xy*-doughnut plus 6.0 mW with regularly focused beam). Pixel size: 30 nm x 30 nm. **d,** Same parameters as in panel a. Data is raw, the colour map is linear.

## Suppl. Figure 6: Protective effect in other fluorophores

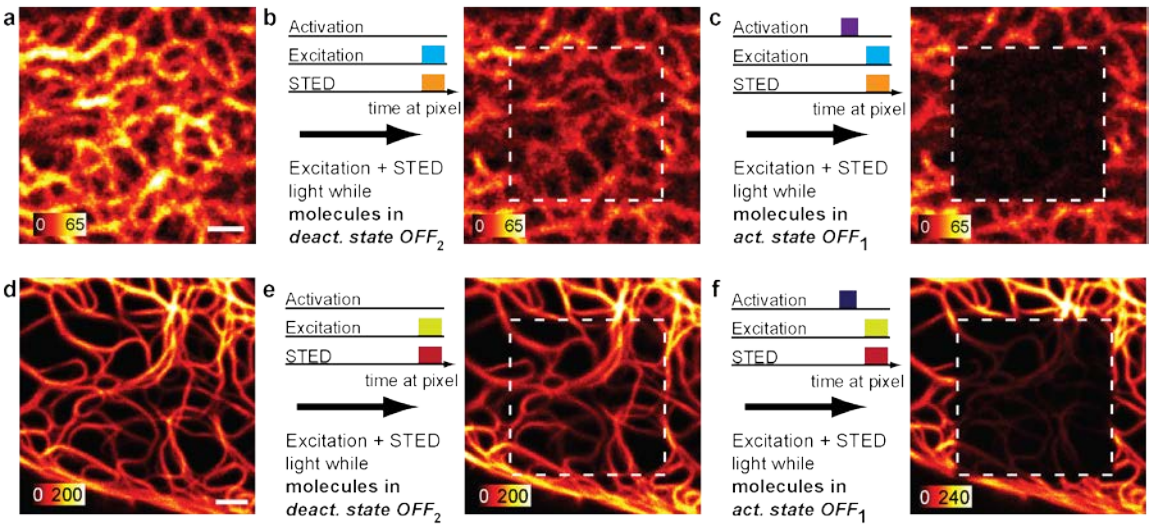


**a,** Confocal image of a living HeLa cell expressing a keratin-Dronpa(M159T) fusion protein[10]. **b,** Confocal image of the same cell after scanning the region indicated by the dotted square with excitation (488 nm) and STED (587 nm) light while molecules resided in the deactivated ("deact.") state, resulting in a low level of photobleaching. **c,** Confocal image after further exposure of the indicated region to the same excitation and STED light dose as before, but with molecules residing in the activated ("act.") state (*i.e.* including an activation light pulse at each scan pixel, as shown in the schematic). Here, pronounced photobleaching is evident. This indicates that, also in this fluorophore, transfer to the deactivated state $OFF_2$ is protective against STED bleaching. **d,** Confocal image of a living HeLa cell expressing a vimentin-rsCherryRev1.4 fusion protein[6]. **e,** Confocal image of the same cell after exposing the region indicated by the dotted square to excitation (560 nm) and STED (775 nm) light while molecules resided in the deactivated state $OFF_2$. **f,** Confocal image after exposing the same region to excitation and STED light with

DOI: 10.1038/NPHOTON.2015.266

the same parameters as before but with molecules residing in the activated state. Again, STED photobleaching is markedly reduced by transfer of molecules to the deactivated state $OFF_2$.
Note that both of these coral-derived fluorescent proteins are unrelated to rsEGFP. Whereas Dronpa emits in the green spectral region, similar to rsEGFP variants, rsCherryRev1.4 emits in the red spectral region.
Scale bars: 1 μm.

Parameters:
**b,c,** Pulse sequence for bleaching: activation: (405 nm, 50 μs, 230 nW); break (10 μs); excitation (488 nm, 40 μs, 0.9 μW) plus STED with *xy*-doughnut (587 nm, 7.3 mW). Pixel size was 20 nm x 20 nm and each region was scanned 5 times. For exposure of molecules in the deactivated state, fluorophores were transferred to $OFF_2$ by irradiation at 470 nm in a larger region and activation light intensity was set to zero in the pulse sequence. Confocal images in panels a-c were smoothed by convolution with a 1.2 pixel wide Gaussian with ImSpector.
**e,f,** Pulse sequence for bleaching: activation (440 nm, 200 μs, 3.7 μW); break (10 μs); excitation (560 nm, 500 μs, 0.4 μW) plus STED with regularly focused beam (775 nm, 17.5 mW); break (10 μs). Pixel size was 20 nm x 20 nm and the region was scanned 5 times. For exposure of molecules in the deactivated state, fluorophores were transferred to $OFF_2$ by irradiation at 590 nm in a larger region and activation light intensity was set to zero. Confocal images were taken with activation at 440 nm and *cw*-excitation at 590 nm.

## Suppl. Figure 7: Images for protected STED and STED series in Fig. 3a

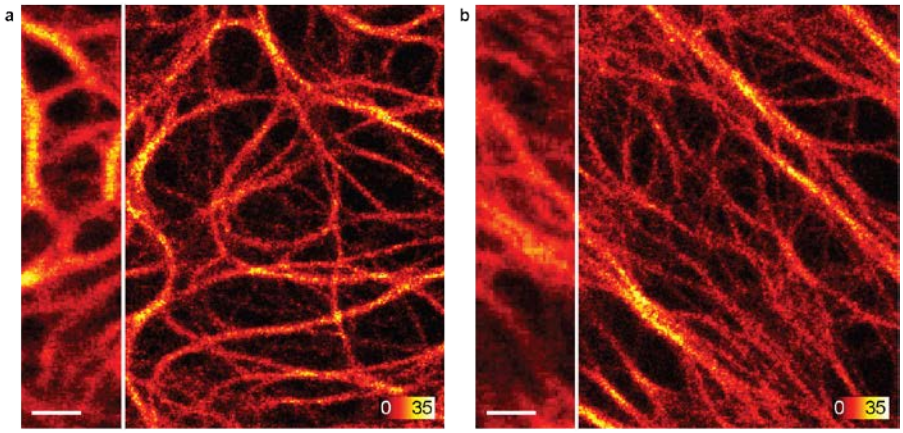


**a,** Protected STED image of a living HeLa cell expressing a keratin-rsEGFP2 fusion protein, taken with the same parameters as in Fig. 3a,b. The left side shows the confocal counterpart. **b,** STED image of a different living HeLa cell expressing keratin-rsEGFP2, taken with the same parameters as in Fig. 3a,b. Imaging parameters for STED and protected STED were adjusted to yield comparable image brightness and resolution with both methods and were chosen to allow recording of several frames also with STED.
Scale bars: 1 μm. Images represent raw data smoothed with a 1.2 pixel wide Gaussian.

## Suppl. Figure 8: Protected STED is robust against variation of parameters

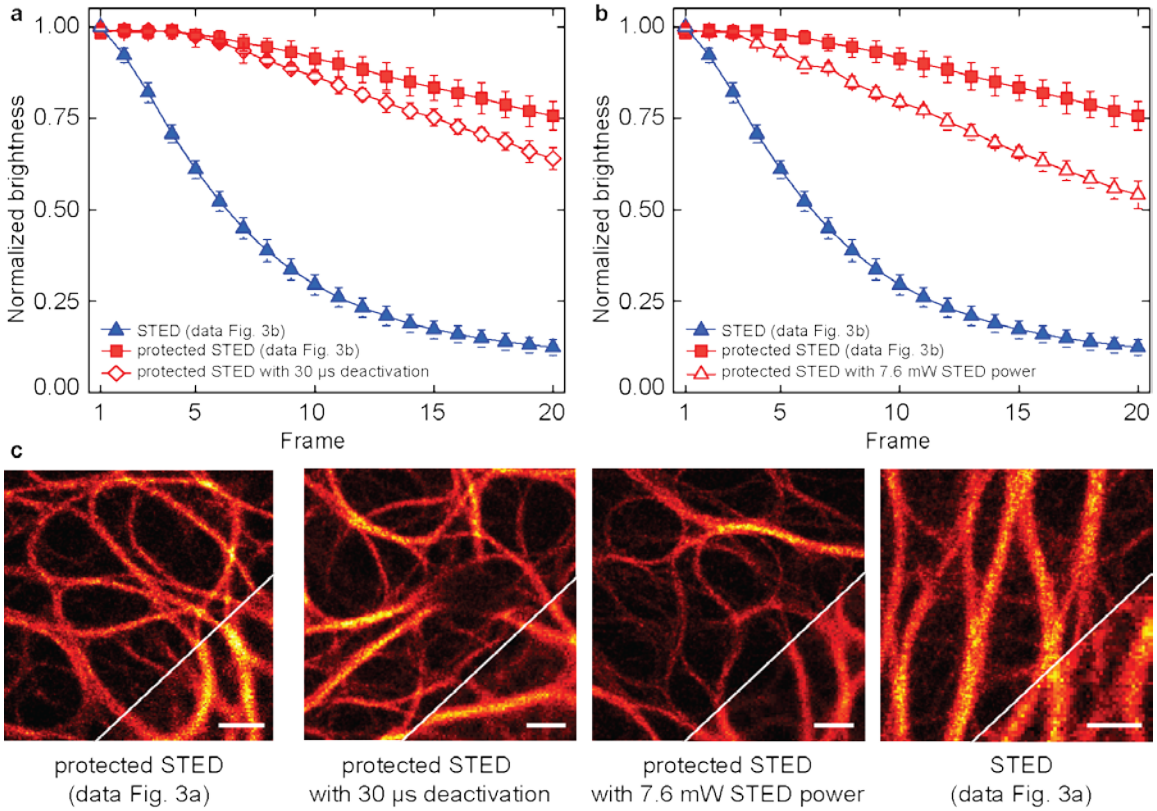


**a,** Repeated protected STED imaging with reduced deactivation time. Image brightness is shown as a function of frame number normalized to the first frame. Here, protected STED was implemented with a shortened deactivation time with respect to Fig. 3b (30 µs as opposed to 350 µs), while keeping image brightness and resolution approximately constant. STED power was increased from 1.5 mW to 3.3 mW in order to compensate for reduced action of reversible photoswitching for generating subdiffraction resolution. Experiments were done in living HeLa cells expressing a keratin-rsEGFP2 fusion protein. While bleaching strongly depends on the chosen imaging parameters, we consistently found that significantly more images could be recorded with protected STED than with plain STED, also with deactivation times shorter than the 350 µs chosen in Fig. 3a,b. For comparison, also the protected STED and STED data from Fig. 3b is plotted. **b,** Protected STED series with the same STED power (7.6 mW) as used in the STED series in Fig. 3b. For a given STED power, considerably more images could consistently be recorded when including the deactivation step. **c,** First frame of representative image series for the different parameter choices in panels a and b. Confocal data is given in the bottom right corners. Scale bars: 1 µm.

Parameters:

**a,** Protected STED with 30 µs deactivation: activation (50 µs, 230 nW); break (10 µs); deactivation with *xy*-doughnut (30 µs, 6.2 µW); excitation (488 nm, 30 µs, 1 µW) plus STED with *xy*-doughnut (587 nm, 3.3 mW); break (6 µs). Mean ± standard deviation from experiments in 5 HeLa cells expressing a keratin-rsEGFP2 fusion protein.

**b,** Protected STED with 7.6 mW STED power: activation (50 µs, 230 nW); break (10 µs); deactivation with *xy*-doughnut (350 µs, 4.4 µW); excitation (488 nm, 40 µs, 1.4 µW) plus STED with *xy*-doughnut (587 nm, 7.6 mW); break (6 µs). Mean ± standard deviation from experiments in 5 cells expressing keratin-rsEGFP2. Protected STED (Fig. 3b): activation (50 µs, 210 nW); break (10 µs); deactivation with *xy*-doughnut (350 µs, 4.4 µW); excitation (488 nm, 40 µs, 2.2 µW) plus STED with *xy*-doughnut geometry (587 nm, 1.5 mW). STED (Fig. 3b): activation (40 µs, 140 nW); break (10 µs); excitation (488 nm, 30 µs, 1.4 µW) plus STED with *xy*-doughnut (587 nm, 7.6 mW). Pixel size in all measurements: 30 nm x 30 nm.

**c,** Colour map in all panels: 0-35 counts.

DOI: 10.1038/NPHOTON.2015.266

## Suppl. Figure 9: T-Rex and RESCue-STED

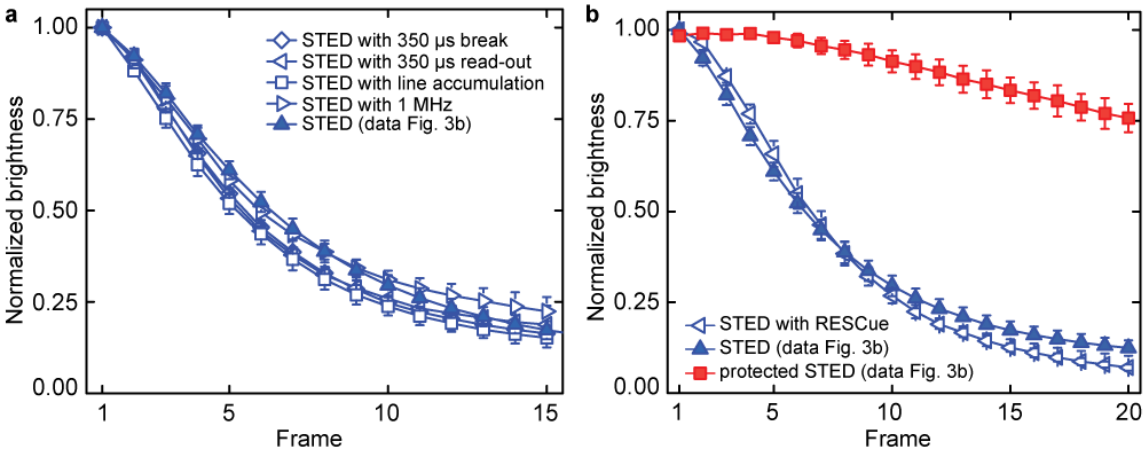


**a,** Image brightness as a function of frame number normalized to the first frame in each series for variations of STED parameters aimed at allowing increased relaxation from bleaching-prone triplet states populated during STED imaging (T-Rex, triplet relaxation). Except for the indicated modifications, parameters were kept constant with respect to Fig. 3b. For comparison, the STED experiments from Fig. 3b are also plotted. Experiments were done on living HeLa cells expressing a keratin-rsEGFP2 fusion protein. We first introduced a break between activation and excitation/ STED periods that was of the same length as the deactivation pulse in protected STED in Fig. 3b ("STED with 350 µs break"). We next reduced the excitation power and concomitantly increased the readout time to 350 µs, thus reducing the excitation probability per unit of time ("STED with 350 µs readout") but collecting approximately the same number of photons. Next, we scanned each line 4 times with 50 µs readout at each pixel with the same STED power but reduced excitation power, leading to 200 µs total readout time per pixel ("STED with line accumulation"). Finally, while keeping the STED pulse energy constant, we applied STED with 1 MHz pulse repetition rate instead of 20 MHz ("STED with 1 MHz"). None of these measures was sufficient to substantially decrease STED bleaching. This indicates that including breaks of µs duration and 20 MHz laser repetition rate, as we did in all STED experiments, was sufficient to take advantage of most of the potential for triplet relaxation. **b,** Comparison of bleaching in STED, RESCue (reduction of state transition cycles)-STED, and protected STED. To test whether RESCue-STED would reduce STED bleaching to a similar degree as protected STED in Fig. 3b, we repeatedly imaged living HeLa cells expressing a keratin-rsEGFP2 fusion protein with RESCue-STED, choosing excitation and STED parameters identical to the STED experiments in Fig. 3b. For RESCue, we used two different decision times (dT) with corresponding lower thresholds (lTh) and an upper threshold (uTh). If either of the lower thresholds was not reached, indicating that no structure of interest was present in a region of subdiffraction extent centred at the scan position, we switched off excitation and STED beams for the remainder of the pixel dwell time. Similarly, light exposure was stopped as soon as the upper threshold was reached and counts were extrapolated to the full exposure time. With the low number of photons collected in each single image from the comparatively dim fluorescent protein labelled structures imaged here, it was not possible to use a short RESCue decision time and at the same time obtain a reliable decision whether or not lasers should be turned off. The shorter the decision time can be chosen, the larger is the bleaching reduction afforded by RESCue-STED. The RESCue-STED curve crosses the STED curve after ~8 frames. This is likely due to the fact that after bleaching fluorophores in the first few frames, the lower thresholds for RESCue were reached more rarely and lasers were shut off more frequently. At pixels where lower thresholds were not reached, the actual count value was replaced by zero, such that dim structures and background signal were rejected from the image.

Parameters:

**a,** Parameters were identical to the STED experiments in Fig. 3b except for the variations noted below.
STED (Fig. 3b): activation (40 µs, 140 nW); break (10 µs); excitation (488 nm, 30 µs, 1.4 µW) plus STED with *xy*-doughnut (587 nm, 7.6 mW). STED with 350 µs break: activation; break (360 µs); excitation plus STED. STED with 350 µs readout: activation; break (10 µs); excitation (350 µs, 110 nW) plus STED (7.6 mW). STED with line accumulation: activation (40 µs, 105 nW); break (10 µs); excitation (50 µs, 130 nW) plus STED; break (6 µs). Each line was scanned 4 times and counts were accumulated, yielding a

total readout time of 200 μs. STED with 1 MHz: activation (40 μs, 105 nW); break (10 μs); excitation (400 μs, 50 nW, 1 MHz repetition rate) plus STED (0.41 mW, 1 MHz repetition rate); break (6 μs). Pixel size: 30 nm x 30 nm. Each series represents mean ± standard deviation from experiments in 3 cells.
**b,** RESCue STED: activation (40 μs, 140 nW); break (3 μs); excitation (30 μs, 1.5 μW) plus STED (7.6 mW) with RESCue-STED decision; break (6 μs). RESCue settings: dT1: 30% of 30 μs, lTh1: 1 count; dT2: 40% of 30 μs, lTh2: 2 counts. Upper threshold: 15 counts. Pixel size: 30 nm x 30 nm. The RESCue-STED series represents mean ± standard deviation from experiments in 4 cells.

DOI: 10.1038/NPHOTON.2015.266

## Suppl. Figure 10: Protected STED imaging of vimentin-rsEGFP2 in living cells

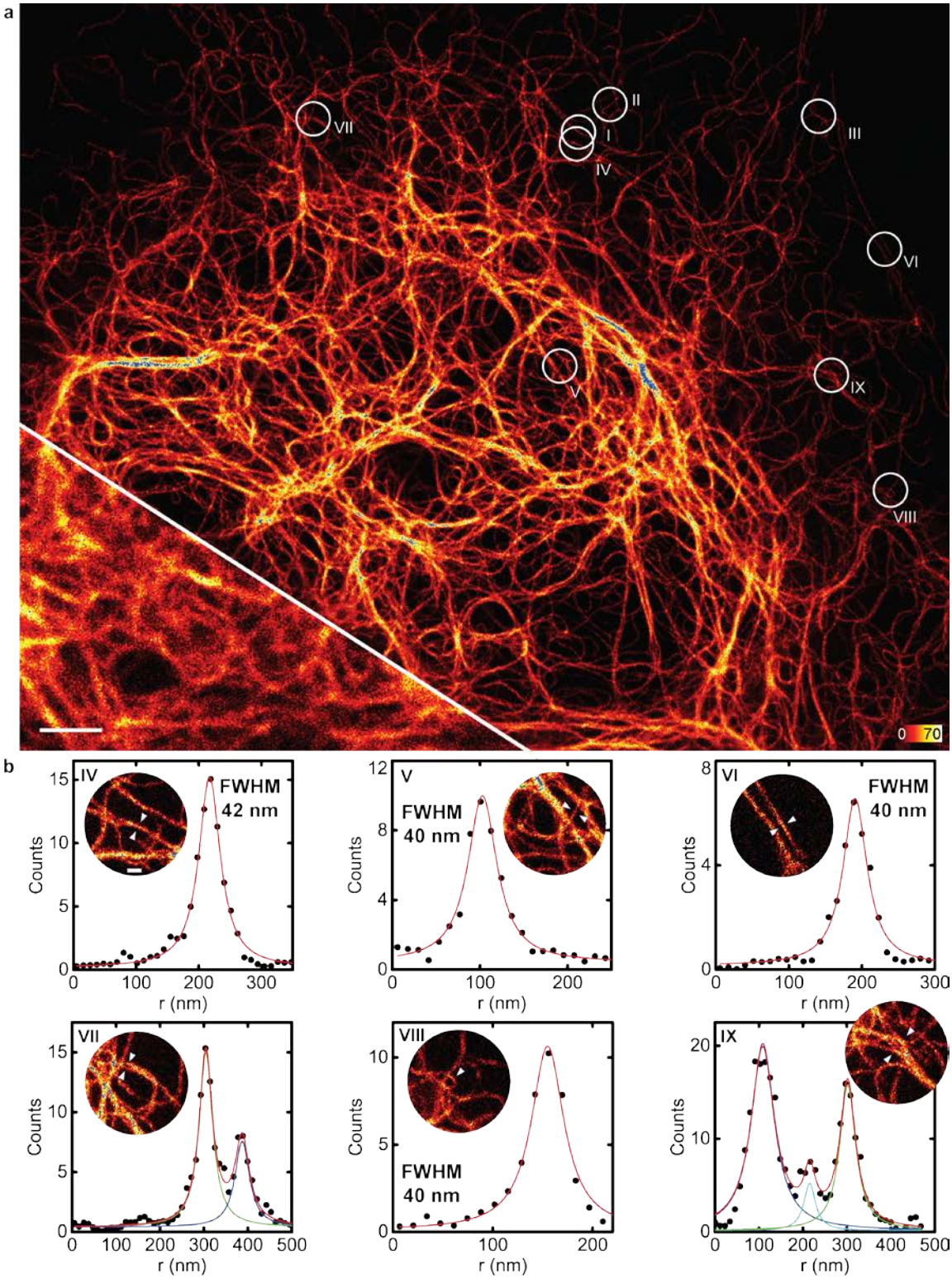


**a,** Same data as in Fig. 4a without smoothing. Bottom left corner: confocal data. Scale bar: 2 μm. Blue colour indicates saturation of the colour map at the brightest structures. **b,** Magnified views of the regions indicated in panel a and line profiles as indicated by the arrowheads. *r*: coordinate along line profile. Regions I-III indicate the regions magnified in Fig. 4b. Scale bar in the first panel: 250 nm, diameter of the

zoomed regions: 1.85 μm. Data are raw, blue colour indicates saturation of the colour map at the brightest pixels. Lorentzian fits yielded full-widths-at-half-maxima (FWHM) of ~40 nm as indicated. The distance between the peaks in region VII is 82 nm, as determined by a double Lorentzian fit. The three peaks in region IX are separated by 107 and 87 nm, respectively. Averaging widths and signal-to-background ratios were as follows, where signal-to-background were determined from the peak and the immediate surroundings of the respective filament:

| Region | Signal-to-background ratio | Averaging width [pixel] | Colour map range [counts] |
|---|---|---|---|
| IV: | 93 | 8 | 0-25 |
| V: | 25 | 10 | 0-35 |
| VI: | 47 | 10 | 0-13 |
| VII: | 38 | 4 | 0-25 |
| | 19 | | |
| VIII: | 137 | 4 | 0-25 |
| IX: | 132 | 4 | 0-25 |
| | 35 | | |
| | 105 | | |

DOI: 10.1038/NPHOTON.2015.266

## Suppl. Figure 11: Protected STED images reveal more detail than RESOLFT images

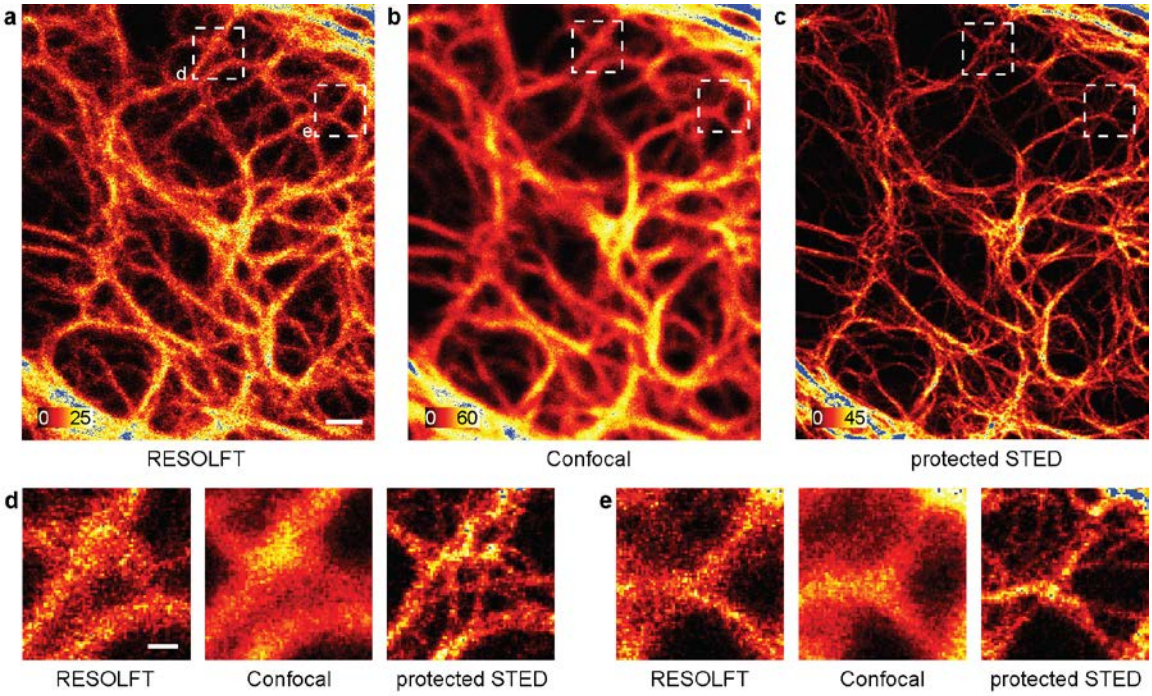


**a,** RESOLFT image of a HeLa cell expressing vimentin-rsEGFP2. Parameters for deactivation in RESOLFT were similar as in previous RESOLFT imaging of cytoskeletal structures[3] with rsEGFP2 and further parameters were adjusted to the sample. The RESOLFT image contains narrow isolated features and displays more detail than the confocal image in panel b. Scale bar: 1 μm. **b,** Confocal image of the same region. **c,** Protected STED image of the same region recorded after the RESOLFT image and with identical parameters as in Fig 4a. **d,e,** Magnified views of the regions indicated in panels a-c for RESOLFT, confocal and protected STED images. Protected STED images reveal considerably more detail than their RESOLFT counterparts. Note that in this living cell, the structures slightly changed between the individual images due to movement of the cell. Scale bar: 250 nm.

Parameters:
**a,** Activation (50 μs, 600 nW); break (10 μs); deactivation with *xy*-doughnut (400 μs, 23.7μW); break (3 μs); excitation (491 nm, *cw*, 10 μs, 9 μW); break (5 μs). Due to *cw*-excitation, no nanosecond time gating was applied.
**c,** Same parameters as in Fig. 4a. Pixel size in all panels: 20 nm x 20 nm. Images represent raw data smoothed with 1.2 pixel wide Gaussian.

## Suppl. Figure 12: Full images from Fig. 4c and comparison of contrast with STED on non-photoswitchable GFP

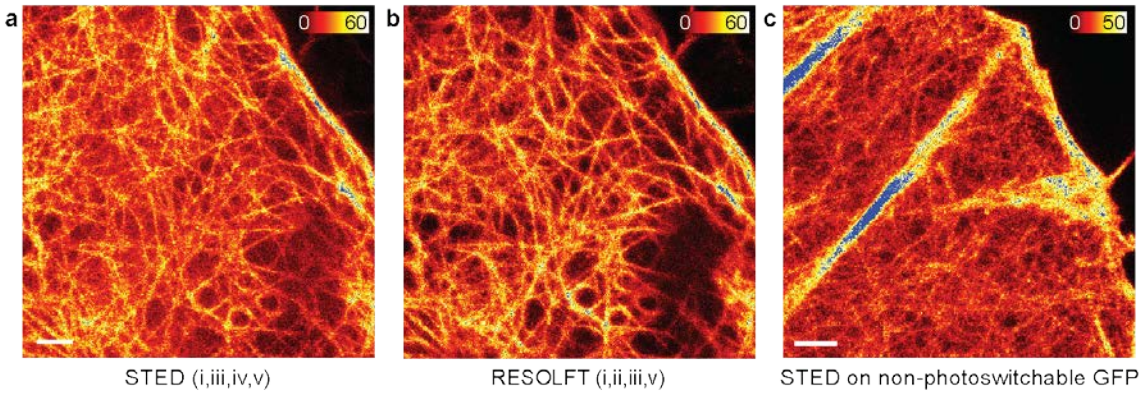


**a,** Full dataset for the STED image in Fig. 4c. **b,** Full dataset for the RESOLFT image in Fig. 4c. **c,** STED image of a living CV-1 cell expressing the actin chromobody (AC) fused to the non-photoswitchable fluorescent protein TagGFP-2. The region is similar to the one chosen in Fig. 4c. Similar to the plain STED image with the photoswitchable actin label AC-rsEGFP(N205S) in Fig. 4c, contrast is limited by cellular background from the dense three-dimensional actin network and potentially also unbound actin label. Scale bar: 1 μm.

Parameters:
**c,** Excitation (488 nm, 1.4 μW) plus STED with xy-doughnut (587 nm, 10.5 mW). Light pulses were applied for 10 μs at each pixel, followed by 5 μs break and each line was scanned 4 times. Detection was time-gated. Pixel size: 20 nm x 20 nm. For labelling, the commercially available actin chromobody GFP plasmid was used (pAC-TagGFP, Chromotek, Planegg). Blue colour indicates saturation of the colour map at bright structures.

## Suppl. Note 1: Image formation with multiple off-states

We present a simplified model for the effective point-spread-function (PSF), $h_{\mathrm{eff}}$, for a combination of STED and reversible photoswitching. The model includes the action of activation, deactivation, excitation and STED with simplified assumptions concerning the effect of deactivation light on reversibly switchable fluorophores. The focal light intensity distributions for driving the individual transitions are given by the respective point spread functions normalized to 1 at the intensity peak: activation: $h_{\mathrm{act}}(x,y,z)$; deactivation: $h_{\mathrm{deact}}(x,y,z)$; excitation: $h_{\mathrm{exc}}(x,y,z)$; STED: $h_{\mathrm{STED}}(x,y,z)$. The light distributions can in principle be obtained by vectorial diffraction theory[11]. However, the main peak of the regularly focused laser beams is well approximated by a Gaussian function in $(x,y,z)$. For the doughnut beams close to the intensity minimum, we assume a quadratic dependence on the radial and axial distances from the intensity minimum $\rho$ and $z$, respectively. In fact, $h_{\mathrm{deact}}$ and $h_{\mathrm{STED}}$ are more complex three-dimensional intensity distributions. For example, an *xy*-doughnut beam in the focal region is essentially an elongated torus (Suppl. Fig. 17) and the intensity gradient along the radial direction shows some variation with the axial coordinate. We assume that molecules are in the deactivated configuration at the beginning of the pulse sequence at each scan position and neglect any memory effect from light action at previous scan positions.

The probability $P_{\mathrm{ON}}$ to reside in the signalling *ON* state after action of the various state transitions is given by the product of the following probabilities: i) for activation, $P_{\mathrm{OFF1}(\leftarrow \mathrm{OFF2})}$; ii) for remaining active after the action of the deactivation pattern, $P_{\mathrm{OFF1}(\rightarrow \mathrm{OFF2})}$; iii) for assuming the fluorescent *ON* state after excitation, $P_{\mathrm{ON}(\leftarrow \mathrm{OFF1})}$; and iv) for remaining on after the action of the STED beam pattern, $P_{\mathrm{ON}(\rightarrow \mathrm{OFF1})}$, such that

$$P_{\mathrm{ON}} = P_{\mathrm{OFF1}(\leftarrow \mathrm{OFF2})}\, P_{\mathrm{OFF1}(\rightarrow \mathrm{OFF2})}\, P_{\mathrm{ON}(\leftarrow \mathrm{OFF1})}\, P_{\mathrm{ON}(\rightarrow \mathrm{OFF1})}. \qquad [1]$$

We assume that activation and excitation probabilities depend linearly on the applied light distribution with the proportionality factors $c_{\mathrm{act}}$ and $c_{\mathrm{exc}}$, respectively. We hence assume that neither of them is driven

DOI: 10.1038/NPHOTON.2015.266

in a saturated mode. Accordingly, $P_{\mathrm{OFF1}(\leftarrow\mathrm{OFF2})} = c_{\mathrm{act}}\, h_{\mathrm{act}}(x,y,z)$ and, with a Gaussian light distribution of full widths at half maximum (FWHM) $\omega_{\mathrm{act,xy}}$ and $\omega_{\mathrm{act,z}}$ in the radial and axial directions, respectively,

$$P_{\mathrm{OFF1}(\leftarrow\mathrm{OFF2})} = c_{act}\, \mathrm{e}^{-4\ln(2)\left(\frac{\rho^2}{\omega_{act,xy}^2}+\frac{z^2}{\omega_{act,z}^2}\right)}, \qquad [2]$$

where $\rho^2=x^2+y^2$.

Analogously, the excitation probability takes the form

$$P_{\mathrm{ON}(\leftarrow\mathrm{OFF1})} = c_{exc} h_{exc}(x,y,z) = c_{exc}\, e^{-4\ln(2)\left(\frac{\rho^2}{\omega_{exc,xy}^2}+\frac{z^2}{\omega_{exc,z}^2}\right)}, \qquad [3]$$

with the radial and axial FWHM $\omega_{\mathrm{exc,xy}}$ and $\omega_{\mathrm{exc,z}}$, respectively.

For the action of pulsed STED[12], we use the well established relation $P_{\mathrm{ON}(\rightarrow\mathrm{OFF1})} = \exp(-\zeta_1\, h_{\mathrm{STED}}(x,y,z))$, where $\zeta_1$ is the ratio of the peak STED light intensity and the saturation intensity $I_S^{\mathrm{ON}\rightarrow\mathrm{OFF1}}$. We approximate the STED light distribution around the minimum with $h_{\mathrm{STED}}(x,y,z) \approx \alpha_1\, \rho^2 + \beta_1\, z^2$, with the wavelength-dependent factors $\alpha_1$ and $\beta_1$ indicating the steepness of the parabolic rise in intensity close to the focal intensity zero along the radial and axial directions, respectively. We further account for the fact that $\zeta_1$ can typically be controlled independently in an experiment for a combination of *xy*-doughnut and *z*-doughnut light distributions, by introducing $\zeta_{1,\mathrm{xy}}$ and $\zeta_{1,z}$. Accordingly, $P_{\mathrm{ON}(\rightarrow\mathrm{OFF1})}$ close to the focus becomes

$$P_{\mathrm{ON}(\rightarrow\mathrm{OFF1})} \approx e^{-(\zeta_{1,xy}\alpha_1\rho^2+\zeta_{1,z}\beta_1 z^2)}. \qquad [4]$$

For reversibly switchable fluorescent proteins, we assume that the probability to reside in the activated state after the deactivation light pulse follows a single exponential decay as a function of deactivation light dose, as in a two-state system where the light-driven transition is much faster than spontaneous relaxation rates. While this is a reasonable assumption at low intensity of deactivation light, photoswitching has a more complex behaviour at high deactivation light intensities in many RSFPs. For deactivation, this dose is the applied intensity integrated over the deactivation time. This implies that deactivation time and intensity can be freely exchanged, which again is only valid in the regime of low photoswitching intensities. In some of our experiments, this assumption is not valid. For example, in fast RESOLFT experiments with short deactivation times (Suppl. Fig. 19), we observe that photoswitching time can in fact not be freely traded for deactivation light intensity.

We further include photoswitching background (*i.e.* residual fluorescence of an ensemble of RSFPs that can be elicited even after deactivation) as a constant probability to reside in the active state $P_{\mathrm{AS,BG}}$ that is independent of light intensities and the spatial coordinates. This is clearly a simplified assumption since as an empirical observation, switching background increases with the intensity driving the deactivating transition[3]. Including photoswitching background yields

$$P_{\mathrm{OFF1}(\rightarrow\mathrm{OFF2})} \approx c'\, e^{-(\zeta_{2,xy}\alpha_2\rho^2+\zeta_{2,z}\beta_2 z^2)} + P_{AS,BG} \qquad [5]$$

with the constant c' for renormalization of the probability and $\zeta_{2,\mathrm{xy}}$ and $\zeta_{2,z}$ giving the ratio between the peak light dose for deactivation and the saturation dose for radial and axial directions, respectively. The factors $\alpha_2$ and $\beta_2$ again give the steepness of the deactivation light distribution around the intensity minimum.

Multiplication of the individual probabilities and including imaging onto the confocal pinhole as a Gaussian of FWHM $\omega_{\mathrm{det,xy}}$ and $\omega_{\mathrm{det,z}}$ in radial and axial directions, respectively, yields the effective PSF $h_{\mathrm{eff}}$. We further combine all (diffraction-limited) Gaussian widths for the radial and axial directions, such that $\frac{1}{\omega_{xy}^2} = \frac{1}{\omega_{act,xy}^2} + \frac{1}{\omega_{exc,xy}^2} + \frac{1}{\omega_{\mathrm{det},xy}^2}$ and $\frac{1}{\omega_z^2} = \frac{1}{\omega_{act,z}^2} + \frac{1}{\omega_{exc,z}^2} + \frac{1}{\omega_{\mathrm{det},z}^2}$, yielding

$$h_{\mathrm{eff}}(x,y,z) = c_{\mathrm{act}}c_{\mathrm{exc}}\left[c' e^{-\left\{4\ln(2)\left[\frac{1}{\omega_{\mathrm{xy}}^2}\rho^2+\frac{1}{\omega_{\mathrm{z}}^2}z^2\right]\right\}} e^{-\{(\zeta_{1,xy}\,\alpha_1+\zeta_{2,xy}\alpha_2)\rho^2+(\zeta_{1,z}\beta_1+\zeta_{2,z}\beta_2)z^2\}} + P_{AS,BG}\, e^{-\left\{4\ln(2)\left[\frac{1}{\omega_{\mathrm{xy}}^2}\rho^2+\frac{1}{\omega_{\mathrm{z}}^2}z^2\right]\right\}} e^{-\{\zeta_{1,xy}\alpha_1\rho^2+\zeta_{1,z}\,\beta_1 z^2\}}\right]. \quad [6]$$

Albeit this model contains a series of simplifications and only a single effect leading to imperfect state contrast for one of the involved off-transitions is explicitly included, it serves to illustrate some of the essential features of protected STED imaging. In the first term of equation [6], both STED and deactivation play an equivalent role and they both contribute to constricting the subdiffraction region of allowed fluorescence. The second term arises from the simple inclusion of imperfect state contrast for one transition, in this case photoswitching background. The imperfect state contrast gives rise to a Gaussian pedestal of diffraction-limited width, but this is counteracted by the action of the other off-transition, in this case STED. Evidently, including effects that lead to imperfect on-/off-contrast in STED would yield additional terms of similar structure as the second term but with the roles of the transitions exchanged. In that case, the deactivating transition counteracts imperfect state contrast in STED and the associated untoward shape of the effective STED PSF, with *e.g.* a diffraction-limited pedestal. For STED, effects compromising state contrast include anti-Stokes excitation by STED light (Suppl. Fig. 15) or spontaneous emission in designated off-regions before full action of the STED light (prominent in *cw*–STED or pulsed STED with long STED pulses, Suppl. Fig. 14).

The first term of equation [6] constitutes the main contribution to the effective PSF. Here, STED and reversible photoswitching play an interchangeable role. They jointly contribute to subdiffraction resolution and their relative contributions can be freely chosen. In addition, the relative contribution to lateral and axial resolution enhancement can be set independently. Importantly, in order to achieve the same resolution, the individual transitions need to be driven less. This is particularly relevant for the STED transition, such that reduced bleaching not only comes from protective transfer to the deactivated state $OFF_2$ but also from a reduction of the necessary STED power to achieve a given resolution. For the deactivating transition, this effect is particularly relevant in fast imaging because it allows using short deactivation times that would not be sufficient to achieve high resolution with the photoswitching transition alone (Suppl. Fig. 19). In that case, transfer to the deactivated state $OFF_2$ primarily serves to protect fluorophores. The structure of the first term corroborates our observation that in protected STED, satisfactory imaging results are achieved within a wide parameter range, including shortened deactivation times, and that there is a large freedom to adjust parameters to a particular imaging situation.

To illustrate the role of the second term of equation [6], it is instructive to set the STED intensity in equation [6] to zero, *i.e.* $\zeta_{1,\mathrm{xy}} = \zeta_{1,z} = 0$. This yields an approximation for the effective PSF in RESOLFT imaging.

$$h_{\mathrm{eff,RESOLFT}}(x,y,z) = c_{\mathrm{act}}c_{\mathrm{exc}}\left[c' e^{-\left\{4\ln(2)\left[\frac{1}{\omega_{\mathrm{xy}}^2}\rho^2+\frac{1}{\omega_{\mathrm{z}}^2}z^2\right]\right\}} e^{-\{(\zeta_{2,xy}\alpha_2)\rho^2+(\zeta_{2,z}\beta_2)z^2\}} + P_{AS,BG}\, e^{-\left\{4\ln(2)\left[\frac{1}{\omega_{\mathrm{xy}}^2}\rho^2+\frac{1}{\omega_{\mathrm{z}}^2}z^2\right]\right\}}\right]. \quad [7]$$

The first term again represents the subdiffraction signal, and is the product of an effective confocal PSF $h_{eff,confocal} = e^{-\left\{4\ln(2)\left[\frac{1}{\omega_{\mathrm{xy}}^2}\rho^2+\frac{1}{\omega_{\mathrm{z}}^2}z^2\right]\right\}}$ and the action of the deactivation transition. However, the second term produces a confocal pedestal in the effective PSF that is not counteracted by any off-transition. Isolated features thus exhibit a narrow central peak, given by the first term. However, the second term limits the achievable contrast between designated on- and off-regions and, with that, may become limiting for the power to resolve closely spaced features. When imaging densely packed fluorescent structures and constricting the central subdiffraction region further and further, a situation may arise where many more fluorophores reside within the volume of diffraction-limited extent around a given scan position than within the subdiffraction region intended for readout. When the specimen is convolved with the effective PSF during image formation, the summation of the confocal pedestals (given by the second term) from fluorophores at nearby positions may overwhelm the signal from the subdiffraction region defined by the first term. The magnitude of the contribution of the second term varies with the RSFP chosen. For

DOI: 10.1038/NPHOTON.2015.266

rsEGFP2, photoswitching background is reported[3] to be around 10% in RESOLFT imaging and is a few per cent in the rsEGFP(N205S) variant (Suppl. Fig. 4,5).

With certain RSFPs, including rsEGFP variants, excitation is coupled to deactivation of fluorophores. This leads to a further effect compromising state contrast in RESOLFT, especially with fast-switching RSFPs that are desirable for high-speed RESOLFT imaging. Off-switching during readout progressively attenuates the first term whereas the second term remains unaffected, thus reducing contrast between the designated on- and off-regions. Modelling this off-switching during readout as a simple exponential decay and integrating over the readout time yields a factor that affects the first term but not the second term of the structure $\tau(I)\left(1-e^{-\frac{t}{\tau(I)}}\right)$, with $\tau(I)$ representing the intensity-dependent time constant for switching the fluorophore off during readout and $t$ giving the readout time. Thus, for prolonged readout periods, state contrast progressively declines. Similarly, in case excitation is coupled to activation of fluorophores, state contrast in RESOLFT is compromised during prolonged readout.

The situation is different in protected STED. Here, $\zeta_{1,xy} \neq 0$ and, in 3D subdiffraction imaging also $\zeta_{1,z} \neq 0$. Therefore, the second term in equation [6] is transformed from a spurious confocal contribution to a subdiffraction signal by the action of the STED doughnut. As pointed out above, the same argument applies to imperfect state contrast created by the STED transition, which is counteracted by the deactivating transition. Similarly, even if fluorophores in the central subdiffraction region are photoswitched to the deactivated state during readout, on/off-contrast is maintained. Hence, superior contrast is achieved between designated on- and off-regions, both in comparison to RESOLFT imaging and STED imaging, which lies at the heart of the synergistic effect between the two off-transitions. Maintaining high on/off-contrast plays a central role for image formation in coordinate-targeted nanoscopy modalities. Interestingly, as the intensity rises quadratically with distance from the intensity minimum, already small values of $\zeta_1$ are sufficient to effectively silence the major (diffraction-limited) contribution from the second term. Hence, small $\zeta_1$ (low STED power) is sufficient to reverse the situation that may arise with single-transition RESOLFT imaging where the central subdiffraction signal is overwhelmed by diffraction-limited background from nearby features.

The model does not include background from structures in out-of-focus planes, arising from the fact that the actual shape of the detection PSF is more complex and confocal sectioning is not perfect, or from unbound label. Furthermore, the real light distributions for the STED and RESOLFT off-transitions deviate from the quadratic approximation, which can lead to imperfect silencing of fluorophores in certain spatial regions. This may *e.g.* become noticeable as sidelobes in the effective PSF in 3D-subdiffraction imaging with single off-transition nanoscopy. In protected STED, the STED and deactivation light distributions have different spatial dependencies, which suppresses any such effects. We observe that adding the photoswitching transition to $OFF_2$ effectively reduces spurious contributions from these various factors in comparison to conventional STED imaging. We take further advantage of the multiplicative action of state transitions when employing two-photon activation selectively in the focal plane.

In a side-by-side comparison of the same structure imaged with RESOLFT and protected STED, we indeed observe that features are clearly separated in protected STED that are not discernible in RESOLFT, indicating higher resolving power (Suppl. Figs. 11, 16, 19).

Taken together, the model captures the following key elements of protected STED imaging: i) STED and reversible photoswitching both contribute to subdiffraction resolution. ii) The contributions of the two transitions can be tuned over a large range with satisfactory imaging results. iii) The individual transitions can be driven more gently for the same optical resolution. iv) The joint action of the two off-transitions yields image quality that is superior to both RESOLFT and STED, i.e. there is a synergy between the two state transitions.

## Suppl. Figure 13: STED and deactivation jointly contribute to subdiffraction image formation

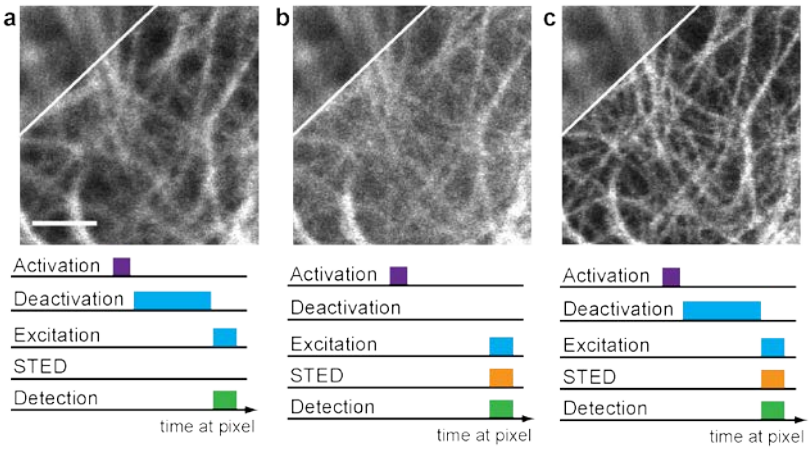


Living CV-1 cell expressing the AC-rsEGFP(N205S) actin label. **a,** RESOLFT image applying activation, deactivation, and excitation pulses. The deactivating transition to $OFF_2$ was driven insufficiently to generate a clearly resolved image of the actin cytoskeleton (i.e. with low $I/I_S$). **b,** STED image of the same region. Here, the STED transition was driven insufficiently to clearly resolve the actin cytoskeleton. **c,** Protected STED image including both deactivation and STED, where each individual transition was driven with the same parameters as before. The actin cytoskeleton is clearly resolved, owing to joint action of the two state transitions. Excitation power was reduced when only one contrast mechanism (reversible photoswitching or STED) was operative (panels a,b) in order to avoid saturation of fluorophores or detectors. Photoactivation parameters were constant throughout. Scale bar: 1 μm.

Parameters:
**a,** Activation (60 μs, 260 nW); break (10 μs); deactivation with *xy*-doughnut (800 μs, 4.6 μW); excitation (488 nm, 70 μs, 0.5 μW).
**b,** Activation; break (70 μs); excitation (70 μs, 0.5 μW) plus STED with *xy*-doughnut (587 nm, 5.8 mW).
**c,** Activation; break (10 μs,); deactivation as in panel a; excitation (70 μs, 2.2 μW) plus STED as in panel b.
Pixel size was 20 nm x 20 nm in all panels. Colour maps are linear with the following scaling: a: 0-110 counts, b: 0-70 counts, c: 0-130 counts, confocal: 0-100 counts. Raw data was smoothed with a 1.0 pixel wide Gaussian.

## Suppl. Figure 14: Effect of time-gating in STED and protected STED images

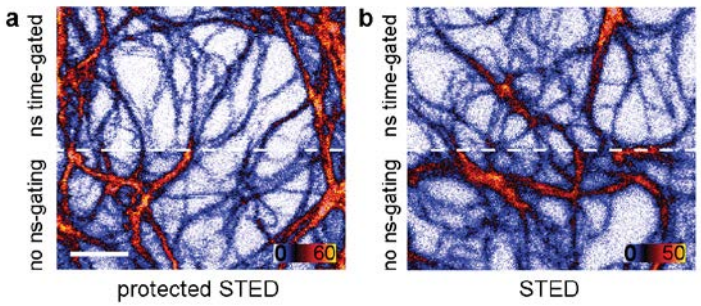


**a,** Living HeLa cell expressing a Vimentin-rsEGFP2 fusion protein imaged with protected STED. The upper half of the image is time-gated on a nanosecond (ns) timescale. In the lower half, time gating was switched off. Time gating has only a minor effect on protected STED images because deactivation of fluorophores in designated off-regions suppresses undesired spontaneous fluorescence emitted before full action of the

DOI: 10.1038/NPHOTON.2015.266

STED pulse. **b,** Vimentin filaments in a living HeLa cell labelled with rsEGFP2, imaged by conventional STED. Again, nanosecond time-gating was turned off in the lower half. In the absence of time-gating, a halo around filaments is apparent from photons spontaneously emitted early after the excitation pulse, reducing state contrast in STED with the ~0.7 ns STED pulses used in our experiments.

Parameters:
**a,** Activation (50 µs, 210 nW,); break (10 µs); deactivation with *xy*-doughnut (350 µs, 4.2 µW); excitation (488 nm, 40 µs, 2.1 µW) plus STED in *xy*-doughnut geometry (587 nm, 7.6 mW); break (6 µs). Each line was scanned twice and counts were accumulated.
**b,** Activation (40 µs, 210 nW,); break (13 µs); excitation (488 nm, 30 µs, 0.6 µW) plus STED in *xy*-doughnut geometry (587 nm, 10 mW); break (6 µs). Each line was scanned twice and counts were accumulated.
Pixel size: 20 nm x 20 nm. Data are raw. Scale bar: 1 µm.

## Suppl. Figure 15: Photoswitching to the deactivated state $OFF_2$ suppresses anti-Stokes excitation by STED light

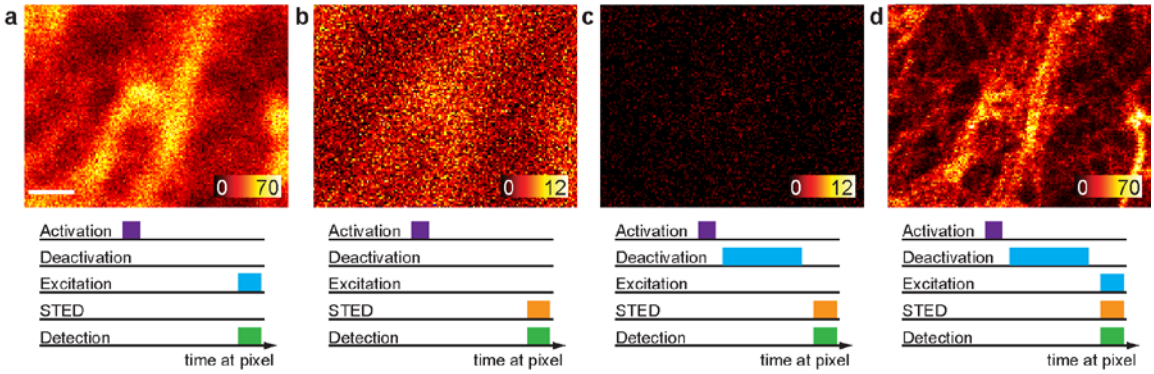


Living CV-1 cell expressing the AC-rsEGFP(N205S) actin label. The pulse sequence at each scan pixel is shown below the corresponding image. **a,** Confocal image. **b,** Excitation by STED light at 558 nm with doughnut beam. This wavelength is shorter than what we generally used for imaging. Accordingly, anti-Stokes excitation, *i.e.* direct excitation by the STED light, was more pronounced. This deteriorates on/off-contrast and leads to a broad pedestal in the effective PSF. The image was taken without excitation light or deactivation light. At 558 nm, rsEGFP(N205S) shows non-negligible excitation by STED light, even at the moderate STED power employed here. **c,** A deactivation pulse (with *xy*-doughnut plus *z*-doughnut) almost completely abolished anti-Stokes excitation by the STED beam. Again, this image was recorded without application of excitation light. **d,** Protected STED image generated by including also excitation light with otherwise identical parameters as in panel c. Actin filaments are more clearly resolved than in panel a and the image is essentially free of background from anti-Stokes excitation by the STED beam.

Parameters:
**b,c,** Same parameters as in panel d but omitting excitation or deactivation pulses as indicated.
**d,** Activation (60 µs, 230 nW,); break (10 µs); deactivation with *xy*-doughnut (1.5 ms, 4.2 µW) together with *z*-doughnut (0.9 µW); excitation (476 nm, 70 µs, 1.6 µW) plus STED in *xy*-doughnut geometry (558 nm, ~2.3 mW). Pixel size: 20 nm x 20 nm. Data are raw. Scale bar: 500 nm.

**Suppl. Figure 16: Protected STED simultaneously provides improved state contrast and improved bleaching**

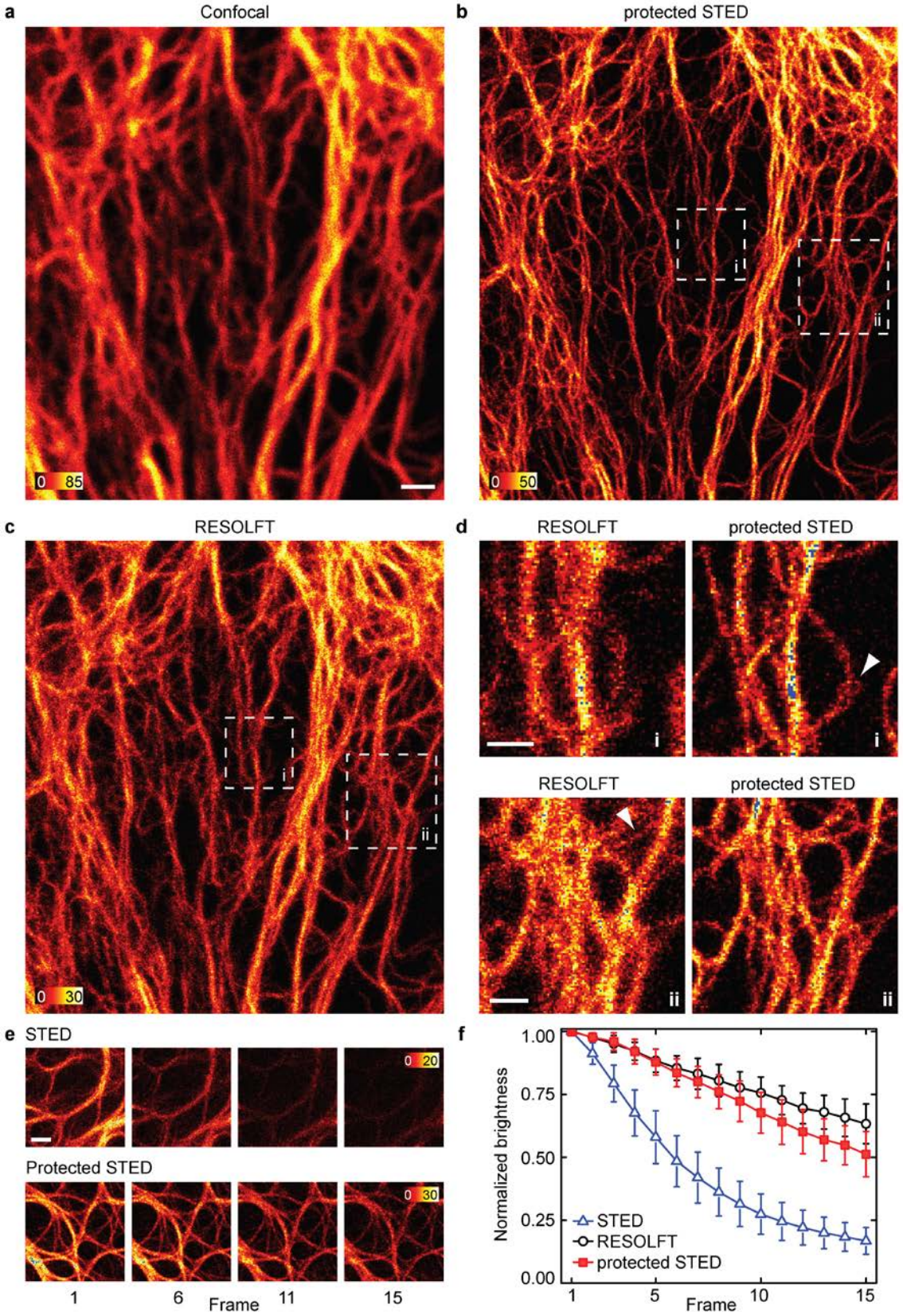


**a,** Confocal image of a living HeLa cell expressing a vimentin-rsEGFP2 fusion protein. Scale bar: 1 μm. **b,** Protected STED image of the same region, recorded after the RESOLFT image in panel c. **c,** RESOLFT

DOI: 10.1038/NPHOTON.2015.266

image of the same region. RESOLFT parameters were adjusted to yield maximum contrast. **d,** Magnified views of the regions indicated in panels b,c. Protected STED images reveal more detail than the corresponding RESOLFT images. In the protected STED image in region (i), peculiar ring-shaped vimentin structures (arrowhead) of sub-diffraction diameter can be discerned. The superior resolution capability in protected STED is evident despite the fact that narrow isolated features can also be discerned in the RESOLFT images (arrowhead in RESOLFT image of region (ii)). Here, the filament indicated by the arrowhead can clearly be followed in protected STED and bends over in a semi-circular shape, whereas this is difficult to ascertain in the RESOLFT image. Note that in this living cell, the structures slightly changed between the individual images due to movement of the cell. Scale bar: 500 nm. **e,** Comparison of bleaching with STED and protected STED in living HeLa cells expressing keratin-rsEGFP2. Parameters for protected STED were identical to the parameters chosen in panel b. Parameters for STED produced a STED image of the same region as in panel b with similar resolution and brightness as in the protected STED image (data not shown). Scale bar: 1 μm. **f,** Image brightness as a function of frame number normalized to the first frame of each series for protected STED, RESOLFT, and STED, recorded with the same parameters as in panels b, c, and e. While protected STED provided clearly superior resolving power compared to RESOLFT, bleaching was similar as in RESOLFT and superior to STED.

Parameters:

**b,** Protected STED: activation (50 μs, 220 nW); break (10 μs); deactivation with *xy*-doughnut (350 μs, 4.4 μW); excitation (488 nm, 40 μs, 2.1 μW) plus STED with *xy*-doughnut (587 nm, 5.1 mW); break (6 μs).
**c,** RESOLFT: activation (50 μs, 210 nW); break (10 μs); deactivation with *xy*-doughnut (400 μs, 8 μW); break (3 μs); excitation (488 nm, 13 μs, 2.2 μW); break (5 μs). Images in panels a-d represent raw data smoothed with a 1.1 pixel wide Gaussian. **d,** Colour map RESOLFT: 0-15 counts; colour map protected STED: region (i): 0-25 counts, region (ii): 0-20 counts. **e,f,** STED: activation (40 μs, 140 nW); break (13 μs); excitation (30 μs, 0.7 μW) plus STED with *xy*-doughnut (10 mW); break (5 μs). Parameters for protected STED and RESOLFT were identical to panels b and c, respectively. Data in panel e represent raw data smoothed with a 1.2 pixel wide Gaussian. Data in panel f represent mean ± standard deviation from experiments in 3 (RESOLFT) or 4 (protected STED, STED) cells**.** Pixel size in all panels: 25 nm x 25 nm.

## Suppl. Figure 17: Protected STED imaging with 3D-subdiffraction resolution in living cells

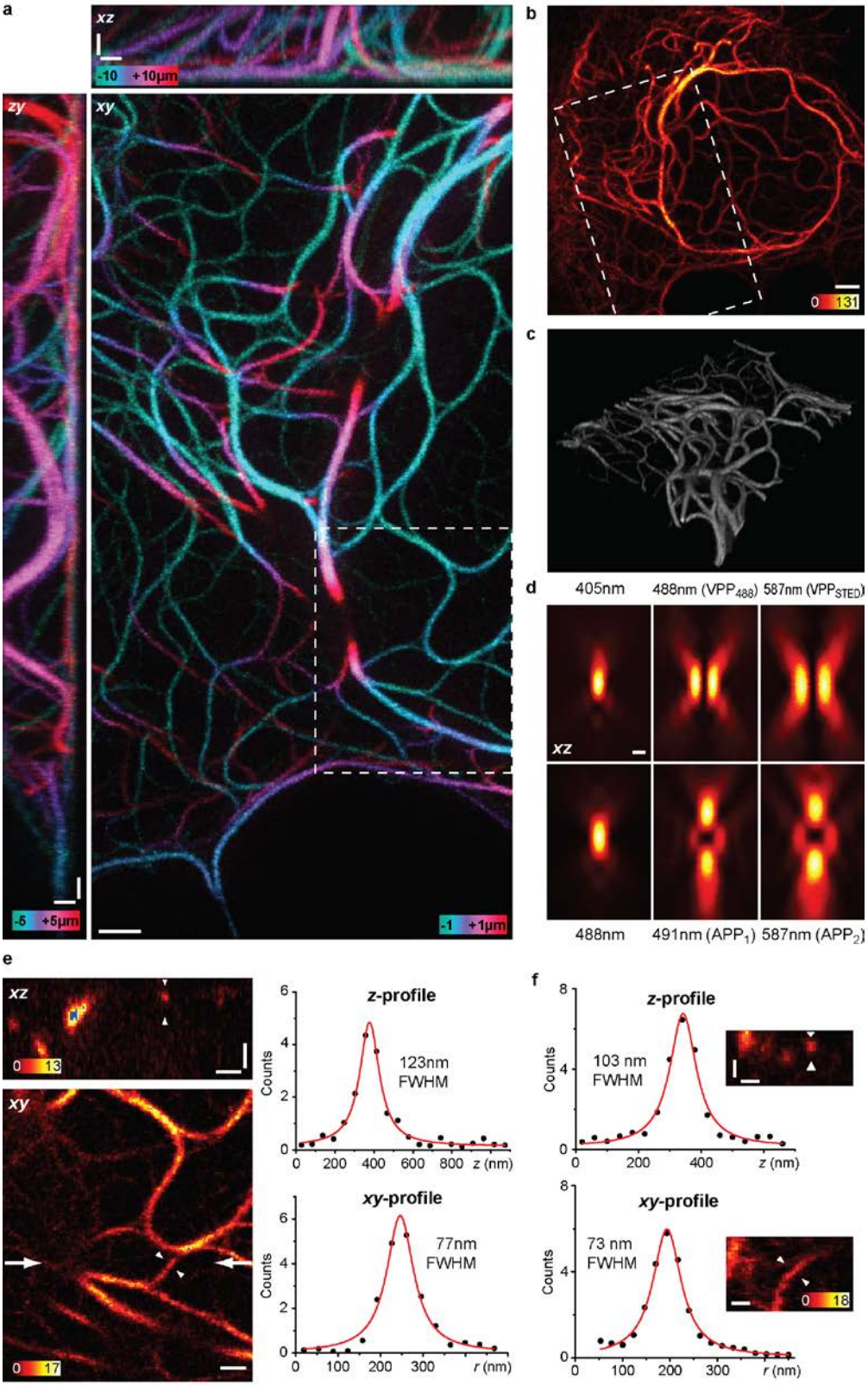


**a,** Three-dimensional arrangement of keratin filaments in a living HeLa cell expressing a keratin-rsEGFP2 fusion protein. The large panel shows an *xy*-view of the 2 µm axial extent of the volume imaged with

DOI: 10.1038/NPHOTON.2015.266

protected STED. Both deactivation and STED were applied with *xy*- and *z*-doughnut beams. The *z*-position is colour-coded. Voxel size was 35 nm x 35 nm x 55 nm along the *x*, *y*, and *z*-directions and the image corresponds to 36 *z*-slices spaced 55 nm apart. The top and left panels show projections along the *y*- and *x*-directions, respectively, and are colour-coded accordingly. The structure is highly three-dimensional, with the filaments spreading out near the base of the cell and forming a basket around the cell nucleus, which is situated in the right part of the *xy*-projection. Scale bars: 1 μm for *xy*-view and 500 nm for *xz*- and *zy*-views. **b,** Confocal overview stack of the same cell. The imaging region for panel a is indicated by the dashed rectangle. The confocal stack was recorded after 3D-subdiffraction imaging of the indicated region, showing that bleaching was moderate during acquisition of the 3D-superresolution stack. Maximum intensity projection of a stack of 6 images spaced by 500 nm in *z*-direction. Scale bar: 2 μm. **c,** Three-dimensional reconstruction of the same dataset as in panel a. **d,** Axial sections of the point-spread functions for the beams employed in 3D-subdiffraction imaging, measured with 80 nm gold beads on a PMT. Activation light at 405 nm and excitation light were regularly focused. The intensity "zeros" of all four patterns for the off-transitions were overlapped in a common location. The naming for the individual patterns in according to the phase masks indicated in Suppl. Fig. 2. Scale bar: 200 nm. **e,** Single *xz*- and *xy*-slices of the volume indicated by the dashed rectangle in panel a. The arrows within the *xy*-section (bottom) indicate the position of the *xz*-section (top). The line profiles represent *z*- and *xy*-profiles of the same filament, as indicated by the arrowheads in the *xz*- and *xy*-sections. The coordinate along the line profile in the *xy*-plane is denoted by *r*. Scale bars: 500 nm. **f,** Line profiles in *z*- and *xy*-direction of a particular filament from a different measurement with denser sampling in the *z*-direction. Voxel size was 35 nm x 35 nm x 40 nm. The stack corresponded to 25 *z*-slices. The insets show a zoomed view of the filament used for the line profiles. The arrowheads indicate the locations of the line profiles. The FWHM of ~100 nm in *z*-direction and ~70 nm in *xy*-direction give an upper bound for optical resolution simultaneously in all three spatial directions for the particular imaging parameters used here. Scale bars: 200 nm.

Parameters and data processing:

**a, c, e,** Activation (50 μs, 230 nW); break (10 μs); deactivation with *xy*-doughnut beam (350 μs, 4.4 μW) and *z*-doughnut (2.1 μW); excitation (488 nm, 40 μs, 2 μW) plus STED at 587 nm with 2.3 mW in the *xy*-doughnut beam and 5.8 mW in the *z*-doughnut beam. Data were recorded in *xzy*-scan mode, *i.e.* with the *y*-direction being the slowest scan axis. Data in panel a were smoothed by convolution with a 1.3 pixel wide two-dimensional Gaussian, first in *xy*- and then in *yz*-direction. The colour lookup table for encoding the third spatial dimension was applied in ImageJ. The three-dimensional rendering in panel c was done with the 3D viewer in ImageJ after smoothing with a 1.5 pixel Gaussian in *xy*- and *yz*-directions. Data in panel e were smoothed with a 1.2 pixel wide Gaussian. Line profiles were generated with ImSpector software from smoothed data without further averaging and fitted with Lorentzian profiles with OriginPro 9.1 software. **b,** Maximum intensity projection of confocal stack with 100 nm x 100 nm x 500 nm voxel, employing only activation and excitation pulses at each voxel. **f,** Activation (50 μs, 220 nW); break (10 μs); deactivation with *xy*-doughnut (350 μs, 4.4 μW) and *z*-doughnut (2.2 μW); excitation (488 nm, 40 μs, 1.3 μW) plus STED at 587 nm with 2.1 mW in the *xy*-doughnut beam and 5.9 mW in the *z*-doughnut beam. The stack was recorded in *xzy*-scan mode. Smoothing and fitting were done as in panel e.

## Suppl. Figure 18: Imaging actin in living cells with 3D-subdiffraction resolution

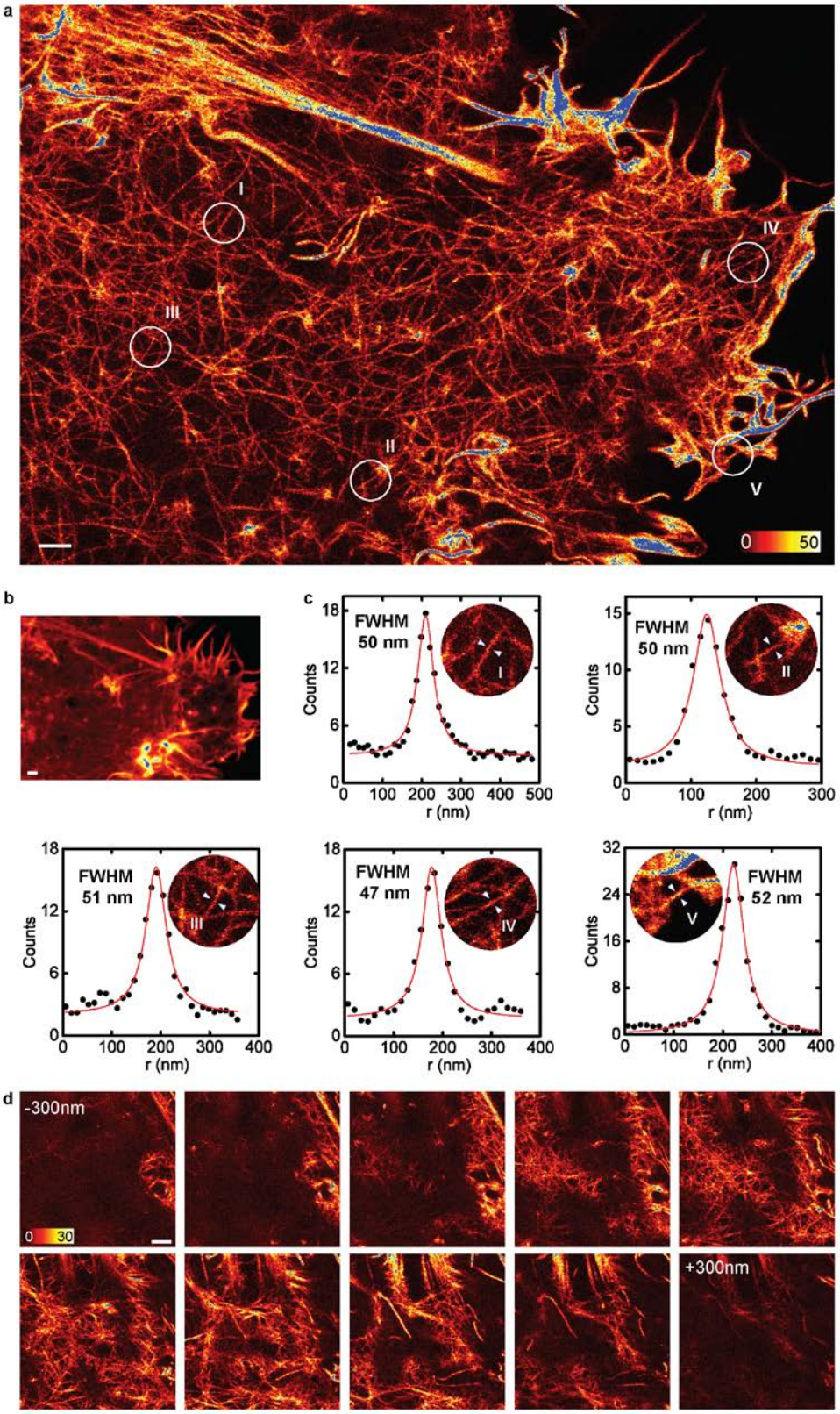


**a,** Same data as in Fig. 5a but without smoothing. Blue colour indicates saturated colour map at thick structures like the stress fibre in the top part of the figure. Scale bar: 1 μm. **b,** Confocal image of the same cell. **c,** Line profiles of the filaments indicated in panel a with Lorentzian fits. *r*: coordinate along line

DOI: 10.1038/NPHOTON.2015.266

profile. **d,** Image stack of a different living CV-1 cell expressing the AC-rsEGFP(N205S) actin label, imaged with 3D-subdiffraction resolution with identical parameters as in Fig 5a. Axial spacing was 61 nm and images show clear differences on this scale of axial distances. Voxel size: 20 x 20 x 61 $nm^3$. Scale bar: 1 μm.

Parameters and data processing:
For imaging parameters, see Fig. 5a.
For panel c, raw data were smoothed in *xy*-direction by convolution with a 1.3 pixel wide 2D-Gaussian. Line profiles were generated with the ImSpector software package on raw data without prior smoothing. An averaging mode was applied that allows setting the width of the region used for line profile calculation. The width was set to 10 pixels. The solid lines represent a fit to the data with a Lorentzian. Fitting was done with the OriginPro software.

## Suppl. Figure 19: Protected STED enables greater detail than RESOLFT for short (<100 μs) pixel dwell time

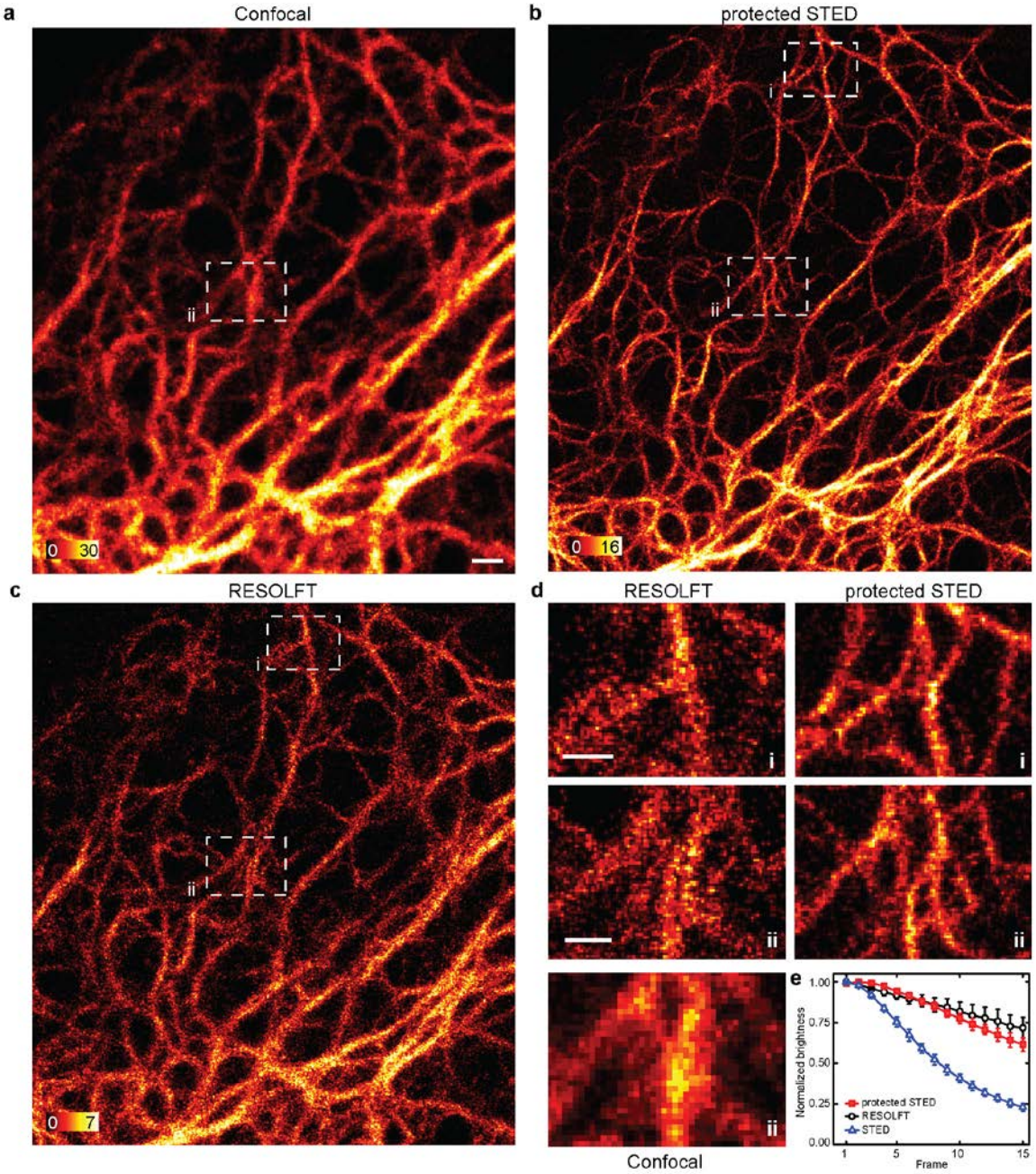


**a,** Confocal image of a living HeLa cell expressing a vimentin-rsEGFP2 fusion protein. Scale bar: 1 μm. **b,** Same region recorded with protected STED with pixel dwell time below 100 μs. Here, deactivation time was shortened to 30 μs and was equal to the STED readout time. **c,** RESOLFT image of the same region recorded with 50 μs deactivation time. Parameters for deactivation in RESOLFT were similar as in previous fast RESOLFT measurements[3]. **d,** Magnified views of RESOLFT and protected STED images for the regions indicated in panels b and c and, for region (ii), also for the confocal image. Scale bars: 500 nm. More details can be discerned in the protected STED than in the RESOLFT image. Total pixel dwell time was slightly larger in protected STED (95 μs) than in RESOLFT (80 μs), due to a 10 μs difference in activation time. We independently confirmed that increasing RESOLFT pixel dwell time to 95 μs with 60 μs deactivation time was not sufficient to improve RESOLFT image quality. Note that in this living cell, the structures slightly changed between the individual images due to movement of the cell. **e,** Normalized

DOI: 10.1038/NPHOTON.2015.266

brightness as a function of frame number for STED, RESOLFT, and protected STED. Parameters for STED were chosen to yield images of similar resolution and brightness as in protected STED.

Parameters:
**b,** Protected STED: activation (30 μs, 610 nW); break (3 μs); deactivation with *xy*-doughnut (30 μs, 8.9 μW); break (1 μs); excitation (488 nm, 30 μs, 1.1 μW) plus STED with *xy*-doughnut (587 nm, 5.1 mW); break (1 μs). The activation time includes a ~10 μs response time of the 405 nm laser.
**c,** RESOLFT: activation (20 μs, 610 nW); break (3 μs); deactivation with *xy*-doughnut (50 μs, 41.4 μW); break (1 μs); excitation (491 nm cw, 5 μs, 3.5 μW); break (1 μs).
**d,** Colour map RESOLFT: 0-6 counts; colour map protected STED: 0-12 counts. Images in panels a-d represent raw data smoothed with a 1.3 pixel wide Gaussian.
**e,** STED: Activation (30 μs, 230 nW); break (4 μs); excitation (30 μs, 0.7 μW) plus STED with *xy*-doughnut (7.9 mW); break (1 μs). Parameters for protected STED and RESOLFT were identical to panels b and c, respectively. Data in panel f represent mean ± standard deviation from experiments in 5 cells expressing a keratin-rsEGFP2 fusion protein. Pixel size in all panels: 30 nm x 30 nm.

## Suppl. Figure 20: Characterization of two-photon activation for protected STED imaging

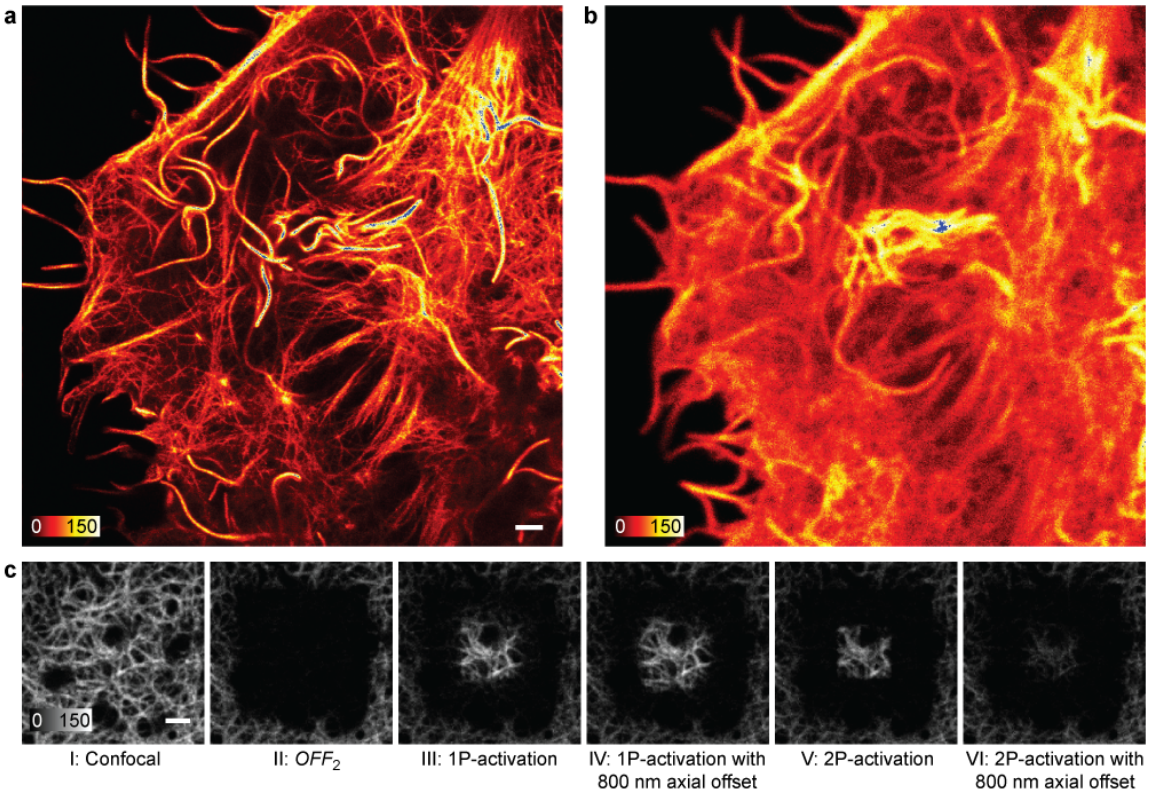


**a,** Raw "protected STED" image of a living CV-1 cell expressing the AC-rsEGFP(N205S) actin label with sub-diffraction resolution both in the focal plane and along the optical axis, employing *xy*- and *z*-doughnuts both for deactivation and STED. 405 nm one-photon (1P-) activation of rsEGFP(N205S) was replaced with 780 nm two-photon (2P-) activation derived from a titanium-sapphire femtosecond laser. Similar to Fig. 5a, the actin network is resolved in a slice of the cell with sub-diffraction axial extent. This shows that two-photon activation is a viable alternative to one-photon activation for driving the $OFF_2 \rightarrow OFF_1$ transition in rsEGFP variants in protected STED imaging. **b,** Confocal image of the same cell as in panel a, employing 1P-activation. **c,** Comparison between 1P-activation at 405 nm and 2P-activation at 800 nm in a living HeLa cell expressing keratin-rsEGFP(N205S). The image series shows confocal scans of the same region after applying various activation regimes as detailed below. Except for the reference image in panel I, no activation light was applied during the confocal scans shown. I: Confocal scan with activation and readout pulses at each pixel. II: Confocal scan after switching molecules in the central region to $OFF_2$ by scanning with 488 nm light. Filaments in the periphery are darker than in panel I

because 488 nm excitation light led to partial deactivation of fluorophores. III: Confocal image after first deactivating in the same region as before and, in a subsequent scan, activating by irradiation of the most central part with 405 nm light. IV: Same as III, but with the focal plane shifted by 800 nm during scanning with 405 nm light. As expected for 1P-activation, molecules were activated essentially equally well in the plane imaged here despite an axial shift during photoactivation. The activated area is slightly larger than in panel III because a larger area is affected by the 405 nm light cone whose focus was placed at an 800 nm axial offset from the plane imaged here. This illustrates that also out-of-focus planes are activated by 1P-activation and can contribute to background signal. V: Same as III, but employing 2P-activation with 800 nm light instead of 1P-activation with 405 nm light. VI: Same axial shift as in panel IV, but with 2P-activation instead of 1P-activation. Brightness in the central region is reduced in panel VI with respect to panel V because of the 800 nm axial shift during the 2P-activation scan. This reflects selective photoactivation of molecules in the (shifted) focal plane. The axial selectivity of fluorophore activation helps to suppress background from out-of-focus planes, which is especially relevant for highly three-dimensional samples. The colour map is linear and identical for all images in panel c. After recording the images shown in the individual panels, confocal images including 1P-activation pulses were taken, creating equal starting conditions before each measurement. Scale bar: 2 μm.

Parameters:

**a,** 2P-activation (60 μs, 3.5 mW); break (10 μs); simultaneous deactivation with *xy*-doughnut (840 μs, 3.6 μW) and z-doughnut (491 nm, 1.9 μW); excitation (488 nm, 100 μs, 2.5 μW) plus 572 nm STED with 7 mW in the *xy*-doughnut beam and 2.7 mW in the *z*-doughnut. Pixel size: 20 nm x 20 nm. Scale bar: 1 μm.

**c,** Parameters for activation with 405 nm light in the central part before recording panels III and IV: power: 110 nW; dwell time per scan pixel: 40 μs; pixel size: 90 nm x 90 nm; 1 scan. Dwell time and pixel size were identical for activation before recording panels V and VI, but 405 nm light was replaced with ~1.5 mW of 800 nm light. No effort was undertaken to compensate for pulse lengthening of the two-photon activation light caused by group velocity dispersion in components of the microscope.

DOI: 10.1038/NPHOTON.2015.266

## Suppl. Figure 21: Maximum intensity projection of the data in Fig. 6

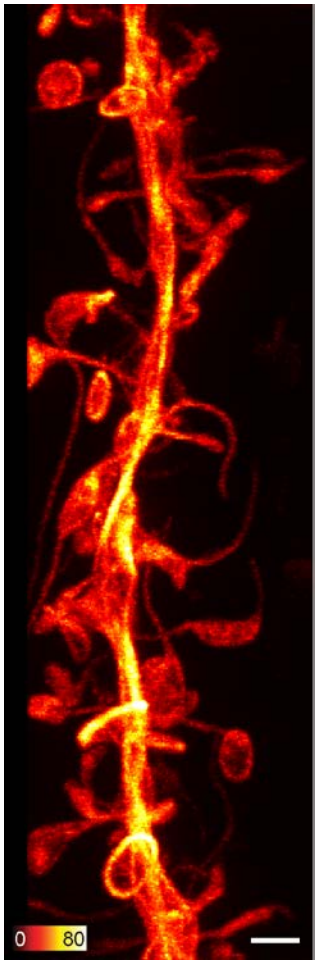


The image represents the same dataset as in Fig. 6 and shows a maximum-intensity projection along the *z*-axis. Raw data was smoothed by convolution with a three-dimensional Gaussian of 1.2 pixel width. Saturation of the colour map at the brightest pixels is indicated in white. Scale bar: 1 μm.

## Suppl. Movie 1: 3D-subdiffraction protected STED imaging in living cells

Animated view of keratin filaments in a HeLa cell expressing a keratin-rsEGFP2 fusion protein recorded with sub-diffraction resolution in all three spatial directions. The movie represents a fly-through along the *y*-direction and represents the same data as in Fig. 5d and panel a of Suppl. Fig. 17. The keratin network is most pronounced near the base of the cell. Individual keratin filaments can be seen to cross multiple *z*-planes.

## Suppl. Movie 2: Time-lapse protected STED imaging of endoplasmic reticulum dynamics

Dynamics of the endoplasmic reticulum in a living CV-1 cell expressing rsEGFP2 fused to an ER-retention signal (KDEL). The movie comprises 500 frames and was recorded at 1 Hz frame rate. The confocal counterpart is shown at the beginning of the movie. STED was applied in *xy*-doughnut geometry. Deactivation was done with both an *xy*-doughnut and *z*-doughnut. The latter served primarily to abolish background signal from out-of-focus planes. Concomitantly, optical resolution along the *z*-axis was moderately enhanced. Pixel dwell time was 85 μs and the times allocated to protective deactivation and to readout including STED were equal (each 30 μs). Image size: 2 μm x 4 μm.

## Suppl. Movie 3: Time-lapse protected STED imaging of peroxisomes in a living cell

Living CV-1 cell expressing a Pex16-rsEGFP2 fusion protein. The movie comprises a total of 70 frames and the confocal counterpart is shown in the beginning. Pixel dwell time was 85 μs, with deactivation and STED both lasting 30 μs. Both the repetition rate of our STED laser of 20 MHz and a finite rise time of the power output of the activation laser on the μs scale limited further reduction of the pixel dwell time. Image size is 5 μm x 10 μm and the resulting frame time was 4.5 s including scanner dead time due to backscanning.

## Suppl. Movie 4: Two-colour time-lapse subdiffraction imaging of endosomes moving along microtubules

Two colour time-lapse nanoscopy combining "protected STED" with conventional STED imaging. Endosomes (colour map fire) were imaged with "protected STED" and can be seen to move along microtubules (green). A rsEGFP2-Rab5a fusion protein was used to label early endosomes. Microtubules were decorated with the fluorescent protein citrine fused to the microtubule binding protein Map2 and imaged with conventional STED. Both fluorescent proteins were excited with a single laser at 476 nm. Separation of rsEGFP2 and citrine signals was achieved by detection in two colour channels and spectral unmixing.

## Suppl. Movie 5: 3D-rendering of a portion of a dendrite in a living hippocampal brain slice

A portion of a dendrite in a living hippocampal brain slice was imaged with subdiffraction resolution in all three spatial directions. The neuron expressed the AC-rsEGFP2 actin label. In this 3D-rendering, a multitude of dendritic spines can be seen to emanate from the dendritic shaft. Same data as in Fig. 6.

## Parameters for Suppl. Movies

**Suppl. Movie 2:**

Activation (590 nW, 20 μs); break (3 μs); deactivation with *xy*-doughnut (4.4 μW, 30 μs) plus *z*-doughnut (3.8 μW); excitation (476 nm, 1.8 μW, 30 μs) plus STED with *xy*-doughnut (587 nm, 2.6 mW). Further breaks for a total of 2 μs were introduced for synchronization. Pixel size: 30 nm x 30 nm. Data are smoothed with a 1.4 pixel wide Gaussian. Colour map nanoscopy: 0-45 counts. Colour map confocal: 0-140. No adjustment of image brightness was applied between individual frames of the movie.

**Suppl. Movie 3:**

Activation (400 nW, 20 μs); break (3 μs); deactivation with *xy*-doughnut (1.8 μW, 30 μs); excitation (476 nm, 1.3 μW, 30 μs) plus STED with *xy*-doughnut (587 nm, 1.3 mW). Further breaks totalling 2 μs were introduced for synchronization. Pixel size: 33 nm x 33 nm. Data are smoothed with a 1.4 pixel wide Gaussian. Colour map nanoscopy: 0-8 counts. Colour map confocal: 0-26 counts. No adjustment of image brightness was applied between individual frames of the movie.

**Suppl. Movie 4:**

Activation (650 nW, 20 μs); break (3 μs); deactivation with *xy*-doughnut (1.8 μW, 30 μs); excitation (476 nm, 1.2 μW, 30 μs) plus STED with *xy*-doughnut (587 nm, 1.3 mW). Further breaks for a total of 2 μs for synchronization. Pixel size: 30 nm x 30 nm. Linear unmixing of the two colour channels was performed with ImageJ. Thereafter, smoothing by convolution with a 2 pixel wide Gaussian was applied. Colour maps: fire 0-28 counts; green 0-14 counts. No adjustment of image brightness was applied between individual frames of the movie.

## Supplementary References

1 Vicidomini, G. *et al.* Sharper low-power STED nanoscopy by time gating. *Nat. Methods* **8**, 571-573 (2011).

2 Chmyrov, A. *et al.* Nanoscopy with more than 100,000 'doughnuts'. *Nat. Methods* **10**, 737-740, (2013).

3 Grotjohann, T. *et al.* rsEGFP2 enables fast RESOLFT nanoscopy of living cells. *eLife* **1**, e00248 (2012).

DOI: 10.1038/NPHOTON.2015.266


4 Urban, N. T., Willig, K. I., Hell, S. W. & Nägerl, U. V. STED nanoscopy of actin dynamics in synapses deep inside living brain slices. *Biophys. J.* **101**, 1277-1284 (2011).

5 Lamesch, P. *et al.* h0rfeome v3.1: a resource of human open reading frames representing over 10,000 human genes. *Genomics* **89**, 307-315 (2007).

6 Lavoie-Cardinal, F. *et al.* Two-color RESOLFT nanoscopy with green and red fluorescent photochromic proteins. *ChemPhysChem* **15**, 655-653 (2014).

7 Willig, K. I., Stiel, A. C., Brakemann, T., Jakobs, S. & Hell, S. W. Dual-label STED nanoscopy of living cells using photochromism. *Nano Lett.* **11**, 3970 - 3973 (2011).

8 Gähwiler, B. H., Capogna, M., Debanne, D., McKinney, R. A. & Thompson, S. M. Organotypic slice cultures: a technique has come of age. *Trends Neurosci.* **20**, 471-477 (1997).

9 DiCiommo, D. P. & Bremner, R. Rapid, high level protein production using DNA-based Semliki Forest virus vectors. *J. Biol. Chem.* **273**, 18060-18066 (1998).

10 Stiel, A. C. *et al.* 1.8 angstrom bright-state structure of the reversibly switchable fluorescent protein dronpa guides the generation of fast switching variants. *Biochem. J.* **402**, 35-42 (2007).

11 Richards, B. & Wolf, E. Electromagnetic diffraction in optical systems. II. Structure of the image field in an aplanatic system. *Proceedings A. Royal Society of London* **253**, 358-379 (1959).

12 Hell, S. W. & Wichmann, J. Breaking the diffraction resolution limit by stimulated-emission - stimulated-emission-depletion fluorescence microscopy. *Optics Lett.* **19**, 780-782 (1994).